

## Journal Pre-proofs

Dense mesopelagic sound scattering layer and vertical segregation of pelagic organisms at the Arctic-Atlantic gateway during the midnight sun

Pierre Priou, Anna Nikolopoulos, Hauke Flores, Rolf Gradinger, Erin Kunisch, Christian Katlein, Giulia Castellani, Torsten Linders, Jørgen Berge, Jonathan Fisher, Maxime Geoffroy

PII: S0079-6611(21)00098-7  
DOI: <https://doi.org/10.1016/j.pocean.2021.102611>  
Reference: PROOCE 102611

To appear in: *Progress in Oceanography*

Received Date: 21 December 2020

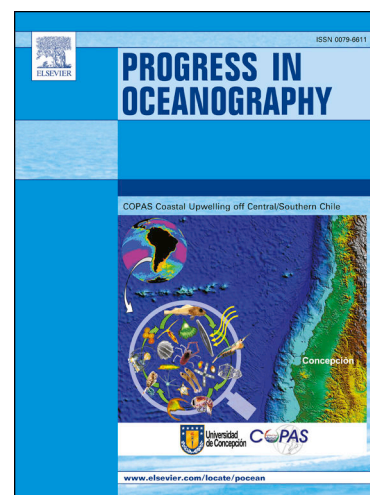
Revised Date: 27 April 2021

Accepted Date: 12 May 2021

Please cite this article as: Priou, P., Nikolopoulos, A., Flores, H., Gradinger, R., Kunisch, E., Katlein, C., Castellani, G., Linders, T., Berge, J., Fisher, J., Geoffroy, M., Dense mesopelagic sound scattering layer and vertical segregation of pelagic organisms at the Arctic-Atlantic gateway during the midnight sun, *Progress in Oceanography* (2021), doi: <https://doi.org/10.1016/j.pocean.2021.102611>

This is a PDF file of an article that has undergone enhancements after acceptance, such as the addition of a cover page and metadata, and formatting for readability, but it is not yet the definitive version of record. This version will undergo additional copyediting, typesetting and review before it is published in its final form, but we are providing this version to give early visibility of the article. Please note that, during the production process, errors may be discovered which could affect the content, and all legal disclaimers that apply to the journal pertain.

© 2021 Published by Elsevier Ltd.



**Dense mesopelagic sound scattering layer and vertical segregation of pelagic organisms at the Arctic-Atlantic gateway during the midnight sun**

Pierre Priou<sup>1\*</sup>, Anna Nikolopoulos<sup>2</sup>, Hauke Flores<sup>3</sup>, Rolf Gradinger<sup>4</sup>, Erin Kunisch<sup>4</sup>, Christian Katlein<sup>3</sup>, Giulia Castellani<sup>3</sup>, Torsten Linders<sup>5</sup>, Jørgen Berge<sup>4,6,7</sup>, Jonathan Fisher<sup>1</sup>, Maxime Geoffroy<sup>1,4</sup>

\*Corresponding author

<sup>1</sup>Centre for Fisheries Ecosystems Research, Fisheries and Marine Institute of Memorial University of Newfoundland, St John's, NL, Canada

<sup>2</sup>Havforskningsinstituttet/Institute of Marine Research, Framsenteret, Tromsø, Norway

<sup>3</sup>Alfred-Wegener-Institut Helmholtz-Zentrum für Polar- und Meeresforschung, Bremerhaven, Germany

<sup>4</sup>Department of Arctic and Marine Biology, The Arctic University of Norway, Tromsø, Norway

<sup>5</sup>Department of Marine Sciences, University of Gothenburg, Göteborg, Sweden

<sup>6</sup>University Centre in Svalbard, Longyearbyen, Norway

<sup>7</sup>Centre for Autonomous Marine Operations and Systems, Department of Biology, Norwegian University of Science and Technology, Norway

Keywords: Mesopelagic, epipelagic, deep scattering layer, hydroacoustics, Arctic Ocean, Arctic-Atlantic gateway, Svalbard

**Highlights**

- Mesopelagic animals formed a deep scattering layer at the Arctic-Atlantic gateway
- Segregation of epi- and mesopelagic animals under sea ice during the midnight sun
- Higher mesopelagic backscattering strength than previously reported in the Arctic
- Link between mesopelagic backscattering strength and Atlantic water circulation

**Abstract**

Changes in vertical and spatial distributions of zooplankton and small pelagic fish impact the biological carbon pump and the distribution of larger piscivorous fish and marine mammal species. However, their distribution and abundance remain poorly documented at high latitudes because of the difficulties inherent to sampling relatively fast-moving organisms in ice-covered waters. This study documents the under-ice distribution of epipelagic and mesopelagic organisms at the Arctic-Atlantic gateway in spring, during the midnight sun period, using ice-tethered and ship-based echosounders. An epipelagic surface scattering layer composed of copepods consistently occupied the top 60 m and was associated with cold polar surface water (mean temperature of  $-1.5^{\circ}\text{C}$ ). A mesopelagic deep scattering layer (DSL), partly composed of fish, persisted between 280 m and 600 m and was associated with modified Atlantic water. Backscattering strength within the DSL was higher than previously reported in the Arctic and north Atlantic, and increased by two orders of magnitude over the continental slope where one of the Atlantic water pathways enters the Arctic Ocean. Mesopelagic organisms did not perform diel vertical migrations. The consistent segregation between copepods at the surface and their predators at mesopelagic depths suggests limited predator-prey interactions during the midnight sun period, even under the ice cover. Predation on copepods by mesopelagic organisms, including fish, could thus be limited to very pulsed events during the seasonal vertical migration of copepods to and from overwintering depths. This suggests that the arctic mesopelagic food web may be decoupled from secondary production in the epipelagic layer throughout most of the year.

## 1. Introduction

Macrozooplankton and small fish inhabit the mesopelagic zone, between 200 and 1,000 m, and play a crucial role in marine ecosystems by linking primary and secondary consumers to higher predators (Naito et al., 2013; Saunders et al., 2019) and contributing to the biological carbon pump (Davison et al., 2013). Mesopelagic organisms form deep sound scattering layers (DSL) that can be detected by hydroacoustic instruments and possibly represent the largest fish biomass of the world's oceans (Irigoiien et al., 2014). As in most deep oceanic basins (Proud et al., 2017), recent investigations revealed that DSL also occur in the Arctic, although at lower acoustic densities than in temperate regions (Gjørseter et al., 2017; Knutsen et al., 2017; Geoffroy et al., 2019; Snoeijs-Leijonmalm et al., 2021).

Globally, about half of the mesopelagic acoustic backscatter undergo diel vertical migrations (DVM; Klevjer et al., 2016). Migrating animals move to the epipelagic layer (0-200 m depth) to feed at night and descend at greater depths to shelter from predators during daytime. While the hunger state of the migrating individual and the trade-off between visual foraging and predation mortality are generally assumed to be the ultimate drivers of DVM (Hays, 2003; Pearre, 2003), other proximate factors such as light, temperature, or oxygen mediate the amplitude of the migrations (Bianchi et al., 2013; Cade and Benoit-Bird, 2015; Norheim et al., 2016). The relative importance of each of these factors vary spatially, but *in situ* irradiance is considered to play an essential role (Røstad et al., 2016). In the Arctic Ocean, pelagic organisms are attuned to strong seasonal changes in irradiance (Berge et al., 2015). For example, most arctic copepods perform DVM when the photoperiod alternates between day and night, in spring and autumn, but the continuous irradiance and the resulting lack of nighttime refuge against visual predators usually stop DVM during the midnight sun period (Blachowiak-Samolyk et al., 2006; Cottier et al., 2006) when large copepods accumulate near the surface (Darnis and Fortier, 2014). DVM of mesopelagic organisms have been reported under the ice at the end of the midnight sun period and when the day-night cycle resumes in late summer, but the amplitude of these DVM remained below the epipelagic zone (Gjørseter et al., 2017).

The vertical segregation between mesopelagic communities and their zooplankton prey during the midnight sun period was suggested to be responsible for the absence of myctophid in northern Baffin Bay (Sameoto, 1989). The photoperiod constraint hypothesis suggests that by suppressing DVM during part of the year, the extreme photoperiod regime prevailing at high latitudes reduces the foraging success of mesopelagic communities and prevent their viable establishment in the Arctic Ocean (Kaartvedt, 2008). Studies later confirmed this hypothesis and showed a strong decrease in mesopelagic biomass toward the pole (Siegelman-Charbit and Planque, 2016; Knutsen et al., 2017). This latitudinal decrease in biomass was attributed to the reduced amplitude of DVM with the poleward increase in nighttime irradiance during spring-summer (Norheim et al., 2016). Theoretical modelling confirmed that the depth of the DSL in the Norwegian Sea could be predicted by *in situ* irradiance (Langbehn et al., 2019). However, observations of the migrating behaviour of the arctic mesopelagic community during the midnight sun period remain scarce, especially under the ice, as previous studies were conducted in late summer, at the end of the midnight sun period and when the Arctic sea ice extent is at its lowest. Because sea ice and snow thickness strongly attenuate light transmittance to the ocean, in particular prior to the summer melt (Perovich, 2005), they could sufficiently reduce under-ice *in situ* irradiance to modify the vertical distribution and migrating behaviour of mesopelagic organisms, similarly to what has been observed for copepods under the ice (Fortier et al., 2001). If mesopelagic animals perform DVM under the ice cover during the midnight sun period, it would keep the epipelagic and mesopelagic zones intertwined in a large part of the Arctic Ocean during that period. In contrast, if continuous segregation persists under the ice, it would greatly limit predator-prey interactions for most of the year.

In June 2017, in the midst of the midnight sun period, we conducted a drift station north of Svalbard over the eastern slope of the Yermak Plateau (> 900 m depth). Ice-tethered and ship-based echosounders recorded the vernal vertical distribution, DVM, and backscattering strength of pelagic organisms under the ice cover. Here, we test the hypothesis that there is no overlap between epipelagic prey and mesopelagic predators under the ice cover in spring, during the midnight sun period. We also investigate potential drivers of the variation in vertical distribution and backscattering strength of epipelagic and mesopelagic organisms.

## 2. Material and methods

### 2.1. Study area

The R/V *Polarstern* remained anchored to an ice floe over the Yermak Plateau, north of Svalbard, from June 3 to 15, 2017 (Fig. 1). The mean sea ice and snow thickness of the ice floe was 1.90 m (Wollenburg et al., 2020) and was representative of the sea ice conditions prevailing in the area (Castellani et al., 2020). During this period, the vessel drifted ca. 100 km over bottom depths ranging from 930 to 1,608 m. The study area, at the northeast Atlantic gateway to the Arctic Ocean, represents a major deep-water connection between the Atlantic and Arctic basins. The West Spitzbergen Current carries warm Atlantic water along the western slope of Svalbard and splits into three branches at the Yermak Plateau; the Svalbard Branch flowing along the northern slope of Svalbard, the Yermak Pass Branch flowing across the Yermak Plateau, and the Yermak Branch flowing around the Plateau (Fig. 1; Athanase et al., 2020). Four main water masses co-occur in the study area: polar surface water (PSW;  $\sigma_0 \leq 27.70$  and  $\theta < 0$  °C), modified Atlantic water (MAW;  $27.70 < \sigma_0 < 27.97$  and  $\theta < 2$  °C;  $\sigma_0 > 27.97$ ,  $\sigma_{0.5} < 30.444$  and  $\theta > 0$  °C), Atlantic water (AW;  $27.70 < \sigma_0 < 27.97$  and  $\theta > 2$  °C), and Arctic intermediate water (AIW;  $\sigma_0 > 27.97$ ,  $\sigma_{0.5} < 30.444$  and  $\theta < 0$  °C; Meyer et al., 2017).

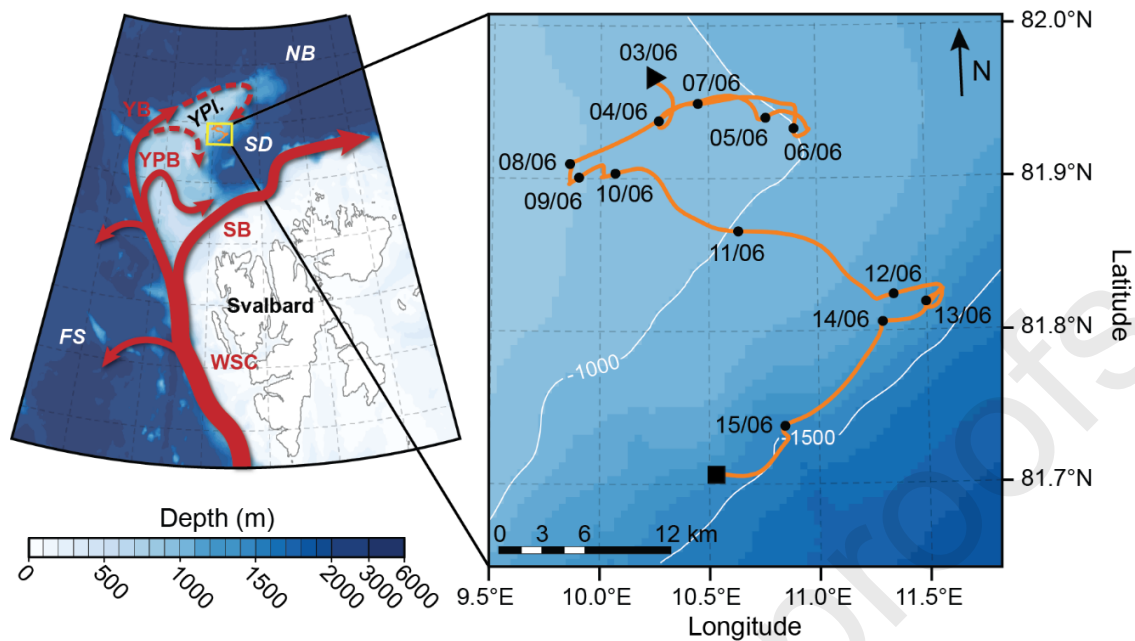


Fig. 1. Bathymetric map of the Yermak Plateau, north of Svalbard, with regional circulation as suggested by Athanase et al. (2020). The yellow rectangle delimits the study area. Red solid arrows show the main pathways of Atlantic water into the Arctic Ocean and the dashed arrow indicates intermittent Atlantic water inflow. The orange line shows the drift trajectory between June 3 (black triangle) and June 15 (black rectangle), 2017. The 1,000 and 1,500 m isobaths are indicated. YPI.: Yermak Plateau; SD: Sofia Deep; NB: Nansen Basin; FS: Fram Strait; WSC: West Spitzbergen Current; SB: Svalbard Branch; YPB: Yermak Pass Branch; YB: Yermak Branch.

## 2.2. Environmental sampling

Temperature, salinity, dissolved oxygen, and fluorescence profiles were measured at least once per day with the shipborne Conductivity-Temperature-Depth system (CTD; Sea-Bird Electronics Inc, SBE-911+ plus) equipped with fluorescence (WETLabs, ECO-AFL/FL) and dissolved oxygen (SBE43) sensors. The temperature and salinity profiles from the ship CTD were used to calculate the speed of sound and absorption coefficients for hydroacoustic calculations. The fluorescence sensor was uncalibrated and only indicated relative values of chlorophyll *a* concentration (a proxy for phytoplankton biomass). Chlorophyll *a* in the top 50 m was also measured with a handheld CTD (Sea & Sun, CTD 75M) equipped with a calibrated fluorescence

sensor (Turner, Cyclops-7) deployed from the sea ice. Additionally, an ice-tethered mooring equipped with three SBE37-IM MicroCAT sensors (Sea-Bird Electronics Inc.) recorded conductivity and temperature at 8, 56, and 141 m depth (and also pressure at 8 m), with a 30-second resolution between June 4 and 16.

A spectral radiation station was installed on the ice floe to measure above and under-ice irradiance. This station consisted of RAMSES hyperspectral radiometers (TriOS GmbH) placed above the ice and at 50 cm below the ice-water interface which measured spectral irradiance (320 to 950 nm). In this study, we used the integrated irradiance over the 320-950 nm range. We also deployed a snow buoy (Met Ocean, Snow Beacon) between June 7 and July 12, which measured snow thickness at the surface of the ice floe.

### **2.3. *Zooplankton sampling***

We sampled zooplankton and under-ice fauna with a plankton net (ROVnet; Wollenburg et al., 2020) mounted on the rear end of a remotely operated vehicle (ROV; Ocean Modules, M500; Katlein et al., 2017). The ROVnet consisted of a polycarbonate frame with an opening of 40 cm by 60 cm, to which a zooplankton net with a mesh size of 500  $\mu\text{m}$  was attached. After each ROVnet deployment, the net was rinsed with ambient seawater to concentrate the sample in the cod end. The ROVnet sampled horizontal profiles in the water below the sea ice. Standard ROVnet profiles were conducted at the ice-water interface, 5 m, and 10 m depth. The distance covered by each profile ranged between 300 and 600 m. Zooplankton were sorted in the laboratory to the lowest possible taxonomic level. We calculated abundances from the zooplankton counts and volume of water filtered by the net, as inferred from the ROV Acoustic Doppler Current Profiler velocity measurements. The ROV also carried a high-resolution video camera used to document the possible presence of fish under the ice.

### **2.4. *Sampling and processing of hydroacoustic data***

Acoustic backscatter was recorded using two ice-tethered single beam Autonomous Zooplankton and Fish Profilers (AZFP; ASL Environmental Sciences) operating at 38, 125, 200, and 455 kHz

and a hull-mounted split beam EK60 (Simrad) echosounder operating at 18, 38, 70, 120, and 200 kHz. The AZFPs deployment was part of the developmental phase of an ice-tethered observatory for plankton and fish (Berge et al., 2016; Zolich et al., 2018). The AZFPs were deployed from June 9 until June 15, whereas the EK60 recorded during the entire drift station (June 3-15). The manufacturer calibrated the AZFPs before deployment, and all the frequencies of the hull-mounted echosounder but the 18 kHz were calibrated after the cruise (June 18) using the standard sphere method (Demer et al., 2015). Here, we show all echograms, including at 18 kHz, but we did not use that frequency for echo-integration because it was not calibrated. Due to the near stationary position of the ship drifting in the ice pack, the ambient noise levels were low, which increased the signal to noise ratio and detection ranges (Fig. S1).

Each AZFP was positioned through holes in the sea ice approximately 100 m away from each other and 100 m away from the ship's echosounder and ADCP mooring to limit acoustic interference. The two AZFPs were moored at 15 m water depth within a stainless-steel frame supported by floats. To limit backscatter from the frame and floats, the AZFPs were mounted with a 15° angle relative to the vertical mooring line. One AZFP faced upward toward the sea ice, and the other faced downward toward the seafloor. The AZFP data were averaged internally with a 38.0 cm (upward-looking unit) or 95.5 cm (downward-looking unit) vertical resolution. Pulse length, ping rate, nominal beam angle, and nominal source-level varied between frequency and between the upward and downward facing AZFP (Table S1).

The ship-based hull-mounted echosounder EK60 was continuously operated during the drift period. The transducers were located at 11 m depth in the ship's hull and pulse length was set to 1.024 ms, the ping rate varied from 0.38 to 0.61 Hz to accommodate for other onboard acoustic instrumentation, and the beamwidth was 11° for the 18 kHz echosounder and 7° for the other transducers (Table S1). The higher transmitted power of the hull-mounted EK60 compared to the AZFP (Table S1) increased the signal to noise ratio and resulted in increased detection ranges for the EK60. The combination of these instruments thus ensonified the water column from ca. 0.5 m under the ice down to 786.0 m depth.

Acoustic data from the AZFPs and EK60 were scrutinized, cleaned, and edited using Echoview 11 (Echoview Software Pty Ltd.). We removed background (minimum 10 dB signal to noise ratio) and impulse noise with Echoview's algorithms (De Robertis and Higginbottom, 2007; Ryan et al., 2015). Little acoustic interference was observed on the upward and downward AZFPs. We echo-integrated the echograms in 10 min long x 1 m deep cells for the upward looking AZFP and 10 min long x 3 m deep cells for the downward looking AZFP and hull-mounted EK60. The mean volume backscattering strength (MVBS in dB re  $1 \text{ m}^{-1}$ ) and nautical area scattering coefficient ( $s_A$  in  $\text{m}^2 \text{ nmi}^{-2}$ ) were exported for each cell. To investigate the vertical migrations of the scatterers, we exported the weighted mean depth (WMD), also called center of mass (Urmy et al., 2012), from 10 min long cells encompassing the full vertical extent of each sound scattering layer at 38 kHz for the EK60 and at 455 kHz for the AZFP data. Backscatter (MVBS and  $s_A$ ) and vertical distribution data were then analyzed in R (version 4.0.3, R Core Team).

Acoustic backscatter (receiver signal strength indicator; RSSI) and water velocities underneath the ice floe were also recorded by an upward looking Acoustic Doppler Current Profilers (ADCP; Teledyne RD Instruments) deployed at 101 m on the MicroCAT mooring line from June 4 to 16. The ADCP recorded data every 3 min in 50 s ensembles with one ping per second and averaged into 4 m depth cells. Data were post-cruise quality assessed with the IMOS Matlab toolbox provided by the Australian Ocean Data Network and Integrated Marine Observing System (AODN IMOS). An additional check was done on occurrences with substantially increased vertical velocities throughout the water column, found to be due to quick changes in tilt at strong winds and high ice-drifting speed (June 7, 10, and 11). For vertical velocity, the affected ensembles were manually removed, and for backscatter, these associated displacements were regarded small enough relative to the data averaging cell size (4 m) to keep. The final valid data range for the ADCP was 15-95 m depth. Further, the ADCP backscatter was extracted from each beam, checked for spurious values (affected ensembles were removed), and converted to mean volume backscattering strength (Gostiaux and van Haren (2010) and references therein). Both backscatter and vertical velocity data were interpolated linearly to 10 min interval and used

to calculate a 24 h ‘model day’ composite averaged over days with good data. For vertical velocity, we used anomalies calculated for each cell by subtracting the record-average vertical velocity prior to synthesizing the composite (Cottier et al. (2006) and references therein). The vertical velocity anomaly 24 h composite was used to check if zooplankton performed asynchronous vertical migrations, as seen by net downward vertical velocities near the surface and net upward vertical velocities below (Cottier et al., 2006).

### 2.5. *Acoustic classification of the scattering layers*

To gain insights into the vertical distribution of different groups of scatterers in the epipelagic zone, we partitioned each echo-integration cell from the ice-tethered AZFPs following the multifrequency selection criteria listed in Darnis et al. (2017). In short, we applied the multifrequency classification on each echo-integration cell to reduce the inherent stochasticity of acoustic data (Korneliussen, 2018), and classified each given cell as being dominated by copepods if  $MVBS_{125\text{kHz}} < MVBS_{200\text{kHz}} < MVBS_{455\text{kHz}}$ , chaetognaths if  $MVBS_{125\text{kHz}} < MVBS_{200\text{kHz}} > MVBS_{455\text{kHz}}$ , or by euphausiids if  $MVBS_{125\text{kHz}} > MVBS_{200\text{kHz}} < MVBS_{455\text{kHz}}$  (Darnis et al., 2017). The maximum range of the 455 kHz transducers limited the range of the dB-differencing analysis to 70 m depth. Although the abundance of zooplankton species varies across regions of Svalbard, e.g., between the Yermak Plateau north of Svalbard and Kongsfjorden on the west coast of Svalbard, both of these areas are influenced by Atlantic water masses and the diversity of zooplankton functional group remains similar (Daase and Eiane, 2007; Darnis et al., 2017). The classification algorithm from Darnis et al. (2017) is therefore applicable to the present study.

We scrutinized the TS of single targets at 38 kHz from the hull-mounted split beam EK60. First, single targets were detected using Echoview’s single-echo detection algorithm for split beam echosounders (method 2) with a maximum beam compensation of 3 dB which only retained single targets close to the beam axis (Table S2). To reduce the computing time, we detected single targets 4 h per day between 0-1, 6-7, 12-13, and 18-19 h from June 4 to 15. Second, we ran Echoview’s fish track algorithm on the single target echograms and extracted single target

tracks (named fish track in Echoview) to reduce the chances of detecting echoes from multiple targets. This algorithm finds single targets that can be tracked over consecutive pings which are assumed to be originating from a single object moving through time and space. As the R/V *Polarstern* was near stationary, we tracked single targets over at least 5 consecutive pings with no missed detection between pings (Table S3). The efficiency of the single target tracking increased with increasing depth due to the widening of the beam. We retained single targets found to be within a maximum horizontal diameter of 2 m (athwartship and alongship) and 1 m range from their position at the previous ping. The algorithm thus excluded animals swimming faster than  $0.77 \text{ m s}^{-1}$ , which is larger than the swimming speed of most mesopelagic animals (Peña et al. (2020) and references therein). We calculated the mean TS and mean depth for each single target track.

## 2.6. *Statistical analyses*

For each sound scattering layer, we used generalized additive models (GAM; Wood, 2017) to explore the relationship between  $s_A$  (used as a proxy for animal density), WMD, and environmental drivers. We log transformed  $s_A$  to meet normality assumptions. Environmental drivers included bottom depth, the vertical extent of water masses of Atlantic origin (MAW and AW), temperature of polar surface water measured at 56 m depth, temperature of modified Atlantic water measured at 141 m depth, time of day, and under-ice downwelling irradiance. To accommodate for the change in irradiance between days, for instance, due to cloud cover or snow melt, we used the interaction of under-ice downwelling irradiance and time of day modeled as a tensor product smooth.

We calculated the degree of collinearity between explanatory variables with the Spearman's correlation coefficient ( $\rho$ ) and used a 0.80 cut-off value. GAMs were fitted with the “mgcv” package in R (version 1.8-33) using a Gaussian distribution with an identity link function. Time of day was modeled with a cyclic cubic regression spline and other explanatory variables were modeled using thin plate regression splines. We estimated the splines with the restricted maximum likelihood (REML) optimization method and limited the number of knots to 5 to

prevent overfitting (Wood, 2017). Models were selected using null space penalization and we included a first order autoregressive error structure in the GAMs to accommodate for autocorrelation of residuals.

### **3. Results**

#### **3.1. *Environmental conditions***

The ice coverage was close to 100 % over the duration of the drift. Four water masses were superposed: polar surface water (PSW) from the surface down to ca. 110 m, modified Atlantic waters (MAW) from 110 m down to ca. 680 m with some intrusions of core Atlantic water (AW) between 120 and 300 m, and Arctic intermediate water (AIW) below MAW (Fig. 2a,b). The vertical distribution of the water masses remained relatively constant in the first part of the drift (June 4-11) with MAW occupying 60 % of the upper 900 m water column. We observed a thickening of the MAW (down to ca. 725 m, occupying 69 % of the top 900 m) after June 11, which coincided with the ice floe drifting southward toward the deeper continental slope (Fig. 1; Fig. 2a,b).

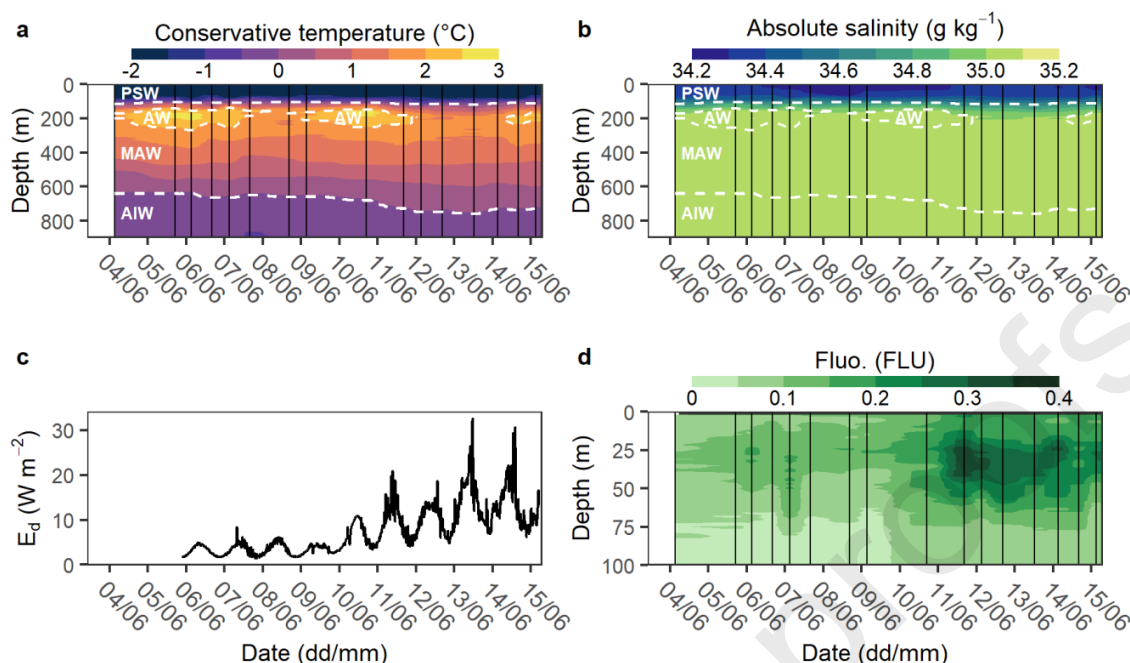


Fig. 2. (a) Conservative temperature and (b) absolute salinity in the uppermost 900 m as measured during the R/V *Polarstern* drift by the ship CTD. Vertical black lines indicate the location of CTD casts and dashed white lines represent the boundaries between water masses. (c) Under-ice downwelling irradiance at 50 cm below the ice-water interface ( $E_d$  in  $W m^{-2}$ ), and (d) fluorescence in the top 100 m (in arbitrary fluorescence units as the sensor was not calibrated). PSW: polar surface water; AW: Atlantic water; MAW: modified Atlantic water; AIW: Arctic intermediate water.

The sun never set below the horizon during the drift, but incident irradiance at the surface of the ice floe displayed a diurnal cycle (Fig. S2a). The under-ice downwelling irradiance at 50 cm below the ice-water interface was ca. 4 % of the irradiance at the surface of the ice floe and exhibited a diurnal pattern with higher irradiance around local midday (UTC + 2h) and lower irradiance around local midnight (Fig. 2c). Thinner snow cover after June 11 increased under-ice downwelling irradiance and the diurnal variation in irradiance, which ranged between 0.7-10.9  $W m^{-2}$  before June 11 and increased to 3.8-32.6  $W m^{-2}$  afterwards (Fig. 2c, S2b). Following that increase in under-ice irradiance, the fluorescence and chlorophyll *a* concentration increased from 0.4-1.0  $mg m^{-3}$  (average of 0.8  $mg m^{-3}$ ) to 0.4-1.8  $mg m^{-3}$  (average of 1.1  $mg m^{-3}$ ) after June 11

(Fig. 2d, S2c). The subsurface chlorophyll *a* maximum was located at 34 m on June 11 ( $1.5 \text{ mg m}^{-3}$ ) and at 22 m on June 15 ( $1.8 \text{ mg m}^{-3}$ ).

### 3.2. *Vertical distribution and backscattering strength of sound scatter layers*

Two distinct acoustic sound scattering layers co-occurred under the ice cover; a shallow epipelagic surface scattering layer (SSL) in the top 60 m and a deep sound scattering layer (DSL) between 280 m and 600 m (Fig. 3). We also observed intermittent scattered patches between the SSL and DSL (Fig 3, S4). The backscatter of the SSL was higher at 455 kHz than at lower frequencies (Fig. 3a), whereas the scattered intermediate patches and DSL volume backscattering strength was stronger at 38 kHz (Fig. 3b), most likely because of lower signal to noise ratio at higher frequencies. We therefore focused the following analyses on the 455 kHz AZFP data for the SSL and 38 kHz EK60 data for the DSL.

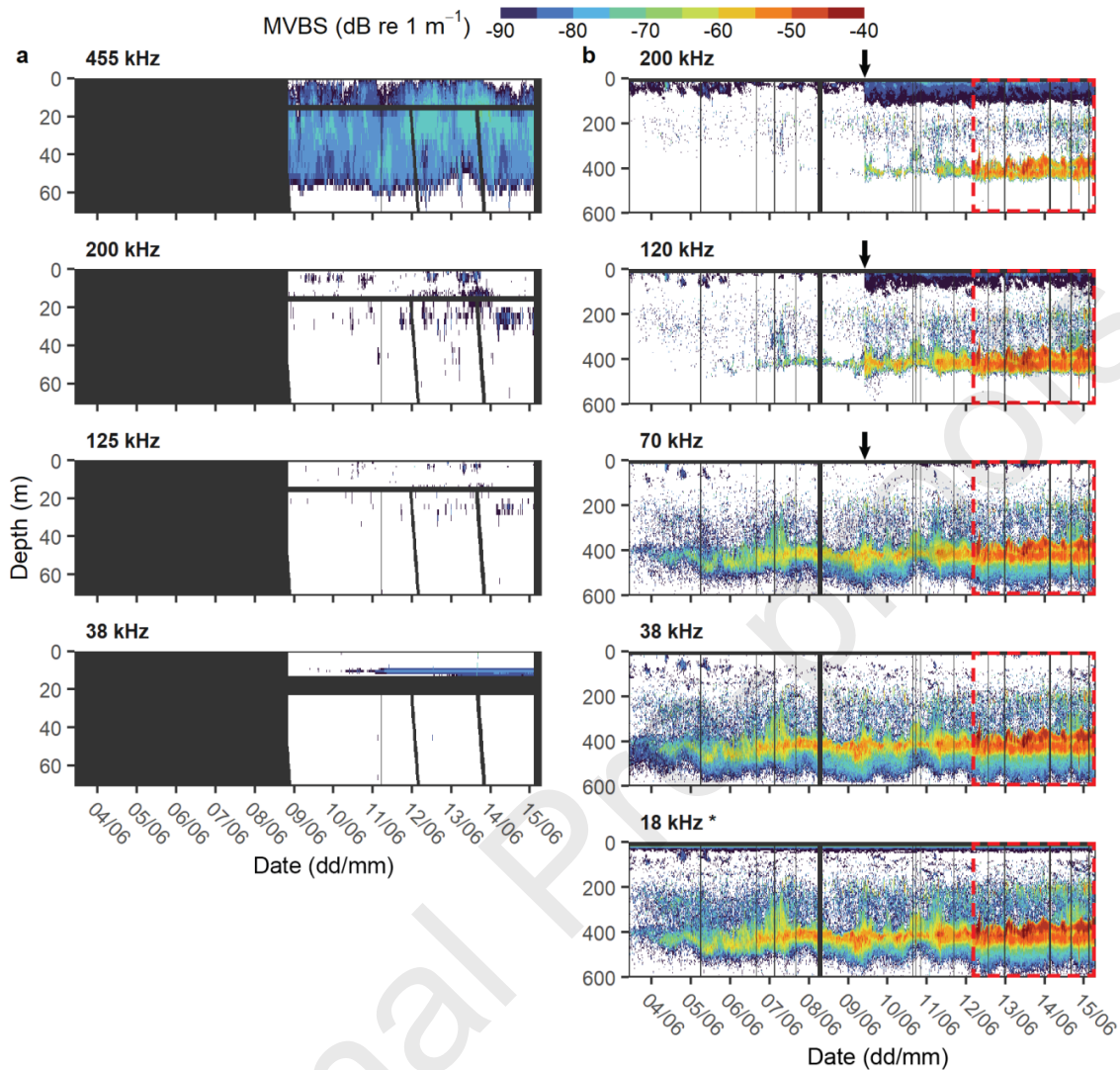


Fig. 3. (a) Composite echograms of denoised mean volume backscattering strength (MVBS in  $\text{dB re } 1 \text{ m}^{-1}$ ) from the upward and downward facing ice-tethered AZFPs at 455, 200, 125, and 38 kHz. (b) Echogram of denoised MVBS from the hull-mounted EK60 at 200, 120, 70, 38, and 18 kHz (\* not calibrated). The dashed red rectangle indicates the south-western part of the drift along the eastern slope of the Yermak Plateau ( $> 1,500 \text{ m}$ ), which coincides with an increase in backscattering strength within the DSL. The black arrows on the EK60 echograms at 200, 120, and 70 kHz on June 9 depicts the change in pulse length which was increased from 0.256 to 1.024 ms at 120 and 200 kHz, and from 0.512 to 1.024 ms at 70 kHz. Areas with bad acoustic data (due to acoustic interference with other instruments, near-field, or dead zone near the sea ice) or with no data are black.

In the epipelagic zone, the SSL had a median WMD of 31 m at 455 kHz and did not follow clear diel vertical migration patterns (DVM; Fig. 4a). However, the lower limit of the SSL detected by the ADCP at 307 kHz was ca. 30 m deeper around midday (ca. 100 m) than at night (ca. 70 m), suggesting small-scale DVM of animals within the SSL (Fig. S3a). These DVM were not detected at 455 kHz because the range of that transducer was limited to the top ca. 70 m. No asynchronous DVM pattern was detected within the SSL (Fig. S3b). The  $s_A$  of the SSL remained relatively stable at a median of 18  $\text{m}^2 \text{nmi}^{-2}$  at 455 kHz before June 11 and increased to a median of 28  $\text{m}^2 \text{nmi}^{-2}$  at 455 kHz afterwards (Fig. 4b).

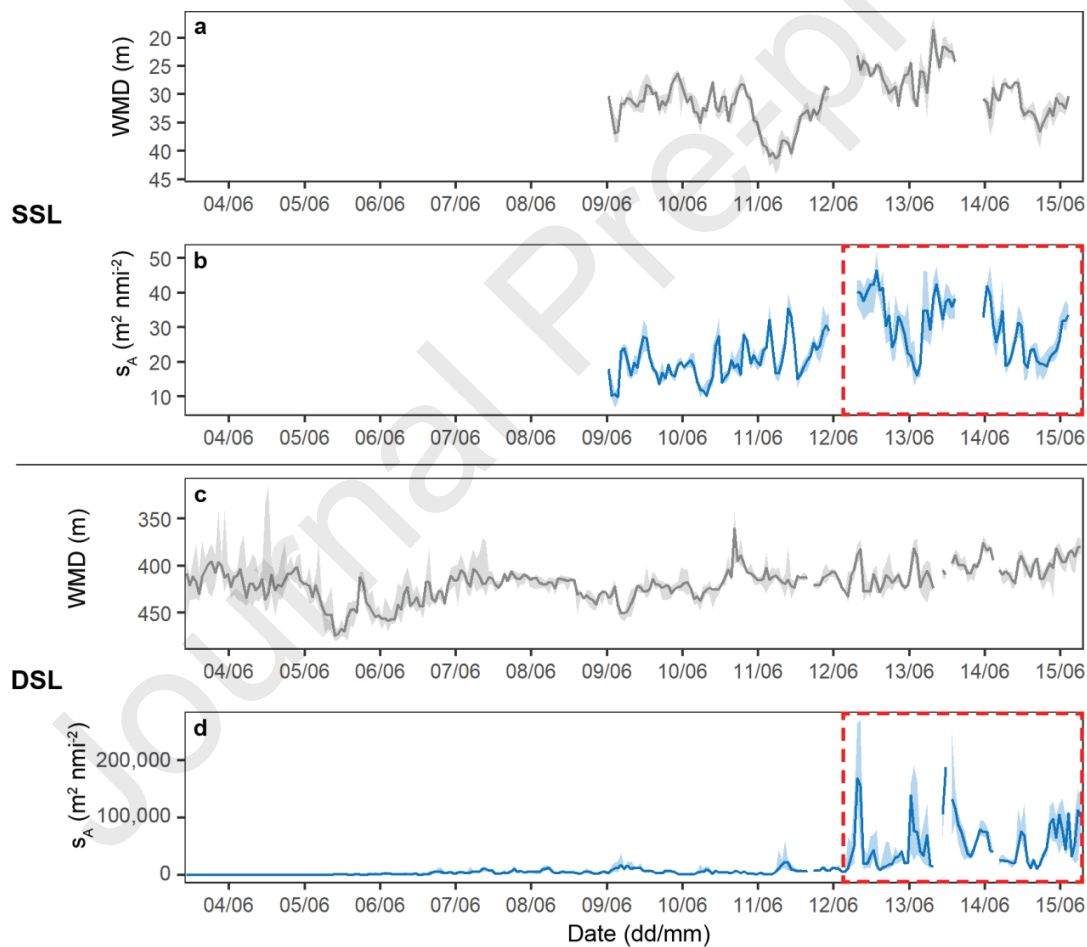


Fig. 4. Weighted mean depth (WMD; grey) and nautical area scattering coefficient ( $s_A$ ; blue) for the (a-b) SSL and (c-d) DSL during the drift station. Solid lines indicate the one-hour moving median, shading indicates the interval where 95 % of the data are located (2.5 and 97.5

percentiles). WMD and  $s_A$  medians were calculated at 455 kHz for the SSL and at 38 kHz for the DSL. The dashed red rectangle indicates the south-western part of the drift along the eastern slope of the Yermak Plateau (bottom depths > 1,500 m), which coincides with an increase in backscattering strength within the SSL and DSL.

The WMD of the DSL remained around 417 m depth ( $\pm 20$  m) over the duration of the drift (Fig. 4c). While animals within the DSL did not conduct DVM, they occasionally migrated vertically, for instance on June 5 and 6 when the WMD was deeper at midday than at midnight. The DSL and scattered intermediate patches were tightly connected, as echoes from the DSL were observed migrating between these two scattering features, but did not conduct large amplitude DVM (Fig. 4c, S4). The backscattering strength of the DSL gradually increased from the beginning of the drift (daily median of  $182 \text{ m}^2 \text{ nmi}^{-2}$  on June 4) until June 11 (daily median of  $7,871 \text{ m}^2 \text{ nmi}^{-2}$ ; Fig. 4d). Thereafter, and until the end of the drift station, it peaked with daily medians ranging between 18,719 and  $56,903 \text{ m}^2 \text{ nmi}^{-2}$ .

### 3.3. Classification of the scatterers

The multifrequency analysis of the AZFP data classified 90 % of the echo-integration cells of the top 70 m as copepods (Fig. S5). No fish were detected near the surface or in the SSL by the ice-tethered AZFP nor the hull-mounted EK60 at 38 kHz. The ROV video footage showed that only few juvenile polar cod (*Boreogadus saida*) were observed closely associated to the ice. *Calanus* spp. (*C. finmarchicus* and *C. glacialis*) dominated the ROVnet catches under the ice with  $182 \text{ ind. m}^{-3}$  on average (Fig. S6). Other abundant epipelagic organisms were the calanoid copepod *Calanus hyperboreus*, hyperiids (*Themisto libellula* and *Themisto abyssorum.*), and typically ice associated gammarid amphipods (mostly *Apherusa glacialis*). Copepods represented on average 91 % of the zooplankton abundance in the ROVnet, which corresponds to the multifrequency classification of AZFP data.

The single targets detected at 38 kHz in the DSL between 200 and 600 m depth had a dominating mode at -36 dB re 1 m<sup>2</sup> and a mode with less targets at -49 dB re 1 m<sup>2</sup> (Fig. S7). These modes indicate that some strong targets, such as swimbladder fish, were associated with the DSL. Weaker targets, such as macrozooplankton or gelatinous zooplankton, were likely present but eluded detection by the TS analysis because of the lower signal to noise ratio at these ranges (Fig. S1).

### 3.4. Environmental factors driving the backscatter intensity of sound scattering layers

The SSL measured by the ice-tethered AZFP at 455 kHz showed that all of the backscatter was contained within the cold and less saline PSW (Fig. 5a). In contrast, the backscatter in the scattered intermediate patches and DSL at 38 kHz from the hull-mounted EK60 was concentrated in waters above 0 °C, in the MAW and AW (Fig. 5b).

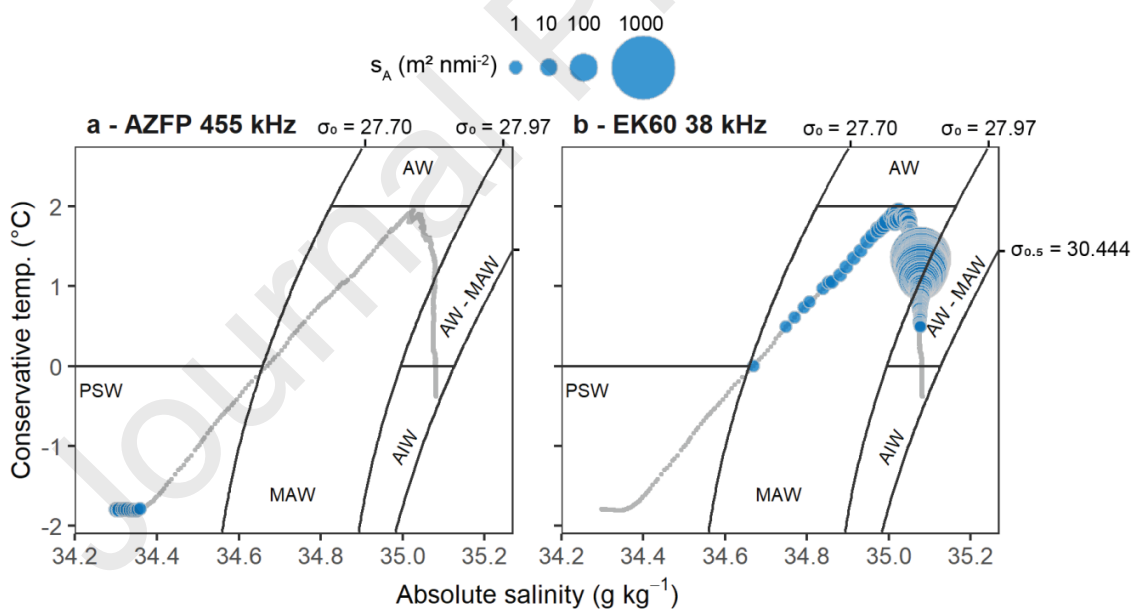


Fig. 5. Nautical area scattering coefficient ( $s_A$ ) overlaid on the average conservative temperature-absolute salinity profiles (grey dots; 3 m vertical resolution). The size of the bubbles is proportional to the  $s_A$  averaged per 3 m depth bin from the (a) ice-tethered AZFP at 455 kHz and

(b) the hull-mounted EK60 at 38 kHz. The isopycnals ( $\text{kg m}^{-3}$ ) used to define the water masses are included. PSW: polar surface water; AW: Atlantic water; MAW: modified Atlantic water; AIW: Arctic intermediate water.

The generalized additive models revealed that bottom depth was the main predictor for both backscattering strength and vertical distribution of the SSL and DSL (Table S4). Bottom depth was positively correlated to the vertical extent of MAW ( $\rho > 0.85$ ,  $p$ -value  $< 0.001$ ) and it was therefore impossible to distinguish the effects from these two covariates. The SSL was deepest (ca. 35 m depth) at 1,250 m bottom depth and the backscatter within the SSL increased with bottom depth (Fig. 6a,b). The DSL remained at ca. 425 m depth where bottom depths were  $< 1,200$  m and ascended to 410 m when the seafloor deepened (Fig. 6c). Similarly, the backscattering strength within the DSL increased in deeper areas (Fig. 6d).

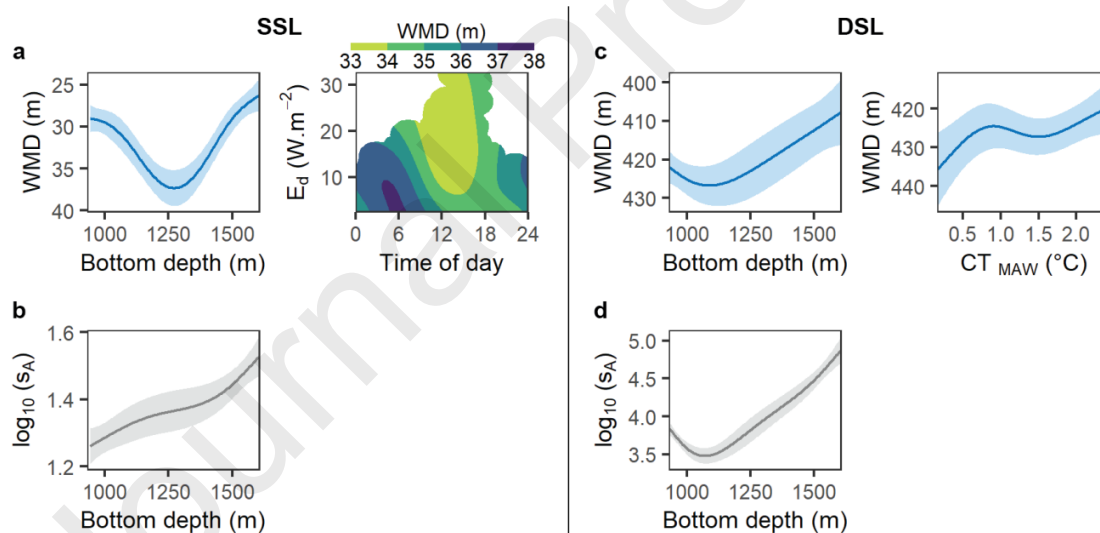


Fig. 6. Significant smooth terms of generalized additive models showing the relationship between environmental drivers for the (a) weighted mean depth (WMD) of the SSL; (b) nautical area scattering coefficient ( $s_A$ ) within the SSL; (c) WMD of the DSL; and (d)  $s_A$  within the DSL. Environmental variables that have been tested included bottom depth, temperature within the PSW ( $CT_{\text{PSW}}$ ), temperature within the MAW ( $CT_{\text{MAW}}$ ), and the interaction between under-ice

irradiance ( $E_d$ ) and time of day (cf. Table S4). Solid lines indicate the estimates of the smooths and shaded areas represent the 95 % confidence interval.

Under-ice irradiance and temperature within the MAW were other significant predictors for the vertical distribution of the SSL and DSL, respectively (Table S4). The SSL was consistently deeper at low irradiance intensities, around midnight, and shallower at high irradiance intensities, around midday (Fig. 6a). This is possibly because copepods remaining outside the range of the 455 kHz during daytime, between 70 m and 100 m, moved within the top 60 m during nighttime (Fig. S3a). The DSL deepened with decreasing temperature of the MAW (Fig. 6c). Overall, the variation in vertical distribution of pelagic organisms remained small and the WMD of the SSL varied between 25 and 40 m and that of the DSL remained between 400 and 430 m.

## 4. Discussion

### 4.1. *Under-ice vertical segregation between epi- and mesopelagic organisms during the midnight sun*

Despite the attenuation of up to 96 % of the surface irradiance by the ice and snow cover, the epipelagic SSL of copepods and the mesopelagic DSL, partly composed of fish, remained vertically segregated throughout the study. Copepods conducted DVM but never descended deeper than 100 m, while the DSL remained in the Atlantic water masses, between 280 and 600 m (Fig. 3). The segregation of epipelagic and mesopelagic organisms during the midnight sun period corroborates earlier observations from the Arctic in ice-free and partly ice-covered conditions at the end of the midnight sun period (Gjørseter et al., 2017). However, contrary to Gjørseter et al. (2017), we did not observe DVM of the mesopelagic community under the ice during the midnight sun period. The light conditions between our study in June, near the summer solstice, and that of Gjørseter et al. (2017) in late August were likely very different and possibly explain this discrepancy. We conducted our study at the start of the melt season with an icescape characterized by few melt ponds and leads, and a relatively thick snow cover (Fig. S2b). The prevailing ice cover (1.90 m thick) and constant illumination did not create an *in situ* light climate favouring large-scale DVM of mesopelagic organisms.

There was no significant relationship between under-ice irradiance and the depth of the DSL (Table S4). Although under-ice irradiance displayed a diurnal cycle, the difference between daytime and nighttime under-ice irradiance remained small (Fig. 2c) and light attenuation by particles including phytoplankton, in particular after June 11 (Fig 2d, S2c), likely resulted in relatively constant *in situ* light levels at mesopelagic depth. Norheim et al. (2016) observed a reduction in DVM amplitude of mesopelagic organisms with increased irradiance at night in the Norwegian Sea and attributed this pattern to the light preferendum hypothesis (Cohen and Forward, 2009). This hypothesis stipulates that animals occupying the mesopelagic realm seek a relatively constant ambient light environment and will adjust their vertical distribution accordingly to remain in their light comfort zone, the optimal environment for foraging while avoiding predation (Røstad et al., 2016). Using a dynamic state variable model validated with acoustic observations along a latitudinal gradient in the Norwegian Sea, Langbehn et al. (2019) confirmed that light, rather than temperature, was the main driver of depth distribution in mesopelagic organisms. The absence of DVM by mesopelagic organisms under the ice during the midnight sun is thus likely resulting, at least in part, from relatively constant *in situ* light levels at mesopelagic depth.

Contrary to the Norwegian Sea, the surface waters of Baffin Bay are characterized by freezing temperatures in summer (Münchow et al., 2015), and Sameoto (1989) suggested that both constant irradiance and freezing temperatures of surface waters were responsible for the absence of myctophid in northern Baffin Bay in summer. A similar combination of factors could have been at play here because subzero temperatures prevailed in the epipelagic zone (mean temperature of  $-1.5\text{ }^{\circ}\text{C}$ ). Therefore, mesopelagic animals could have also avoided surface waters because of thermal stress, in addition to constant irradiance. Moreover, contrary to other regions such as the Norwegian Sea, the mesopelagic fish assemblage at the Arctic-Atlantic gateway is not dominated by lanternfish but rather by juveniles of demersal species such as polar cod, beaked redfish, Atlantic cod, and haddock (Knutsen et al., 2017; Geoffroy et al., 2019). Occasionally, large Atlantic cod ( $> 50\text{ cm}$ ) are observed foraging within the DSL over the Fram Strait and northern Svalbard (Ingvaldsen et al., 2017; Gjørseter et al., 2020). Except for polar cod, these species are not well adapted to freezing temperatures and would generally avoid the

subzero temperatures of the epipelagic zone. Polar cod, on the other hand, is adapted to subzero temperatures and individuals can be found under the ice (David et al., 2016), but most adult polar cod remain in warmer Atlantic waters, at least in the Beaufort Sea (Geoffroy et al., 2011, 2016; Crawford et al., 2012).

#### 4.2. *Ecological implications of the vertical segregation of pelagic organisms*

Despite the importance of copepods as lipid-rich prey for fish within the DSL (e.g., Geoffroy et al., 2019), continuous vertical segregation limited predator-prey interactions between mesopelagic organisms and epipelagic copepods during the midnight sun. Hence, feeding on large copepods, such as *C. glacialis*, *C. finmarchicus*, and *C. hyperboreus*, by mesopelagic fish is likely limited to early spring and fall in the Arctic during the seasonal vertical migration of *Calanus* (Fig. 7). Our findings thus partly support the photoperiod hypothesis, which explains the lower abundance of mesopelagic fish at higher latitudes by inferior feeding conditions imposed by the extreme light climate (Kaartvedt, 2008). When avoiding the strong light and freezing temperatures of the upper water column, mesopelagic organisms lose safe access to feed on lipid-rich prey at night. Some fish species may thus experience insufficient feeding conditions to survive (Norheim et al., 2016).

In fall, the day-night cycle increases the DVM amplitude of both mesopelagic organisms (Gjøsæter et al., 2017) and copepods (Daase et al., 2016), which then overlap vertically. This is also the period when large copepods start descending to overwintering depths after filling their lipid sacs by grazing on phytoplankton, and they thus represent lipid-rich prey for their predators (Falk-Petersen et al., 2009). By looking at the fatty acid trophic markers of mesopelagic organisms in the region, Geoffroy et al. (2019) confirmed that the mesopelagic food web is based on *Calanus* in early autumn. In winter, after large *Calanus* spp. descend to overwintering depths below the DSL (Dale et al., 1999; Hirche et al., 2006), mesopelagic organisms rather feed on euphausiids (e.g., *Thysanoessa* spp.; Geoffroy et al., 2019). In spring, the return of diapausing copepods and copepod eggs from deep overwintering depths to surface waters (Darnis and Fortier, 2014) could also provide a valuable food source for the mesopelagic fishes surviving at

high latitudes. During both winter and summer, when large copepods are not ascending to or descending from the epipelagic layer, these fishes must feed on other prey, such as macrozooplankton (e.g., *Themisto* spp.), or mesopelagic copepods (e.g., *Metridia longa* or *Paraeuchaeta glacialis*; Kosobokova and Hopcroft, 2010). Although the species composition of the scattered intermediate patches is unknown, they were seen at times in close connection with the DSL and could represent another important food source (Fig. S4).

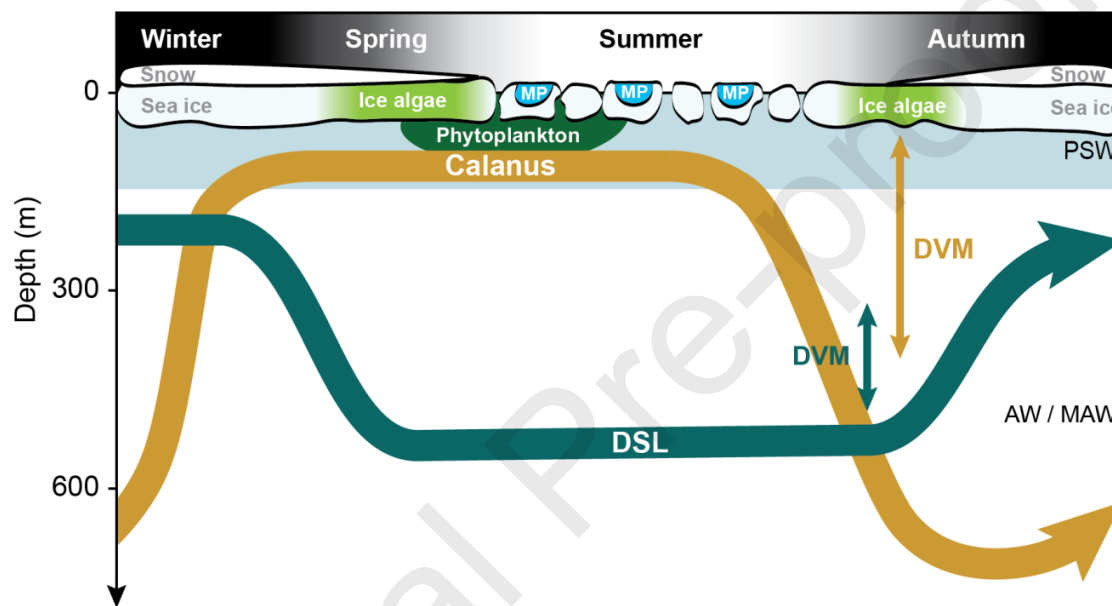


Fig. 7. Schematic of the annual vertical distribution of the mesopelagic deep scattering layer (DSL) and *Calanus* spp. at the Arctic-Atlantic gateway. Based on Gjørseter et al. (2017), Geoffroy et al. (2019), and the present study. Occurrence and relative amplitude of diel vertical migrations (DVM) are represented by vertical arrows. PSW: polar surface water; AW / MAW: Atlantic water / modified Atlantic water; MP: Melt pond.

#### 4.3. *High backscattering strength of the DSL at the Arctic-Atlantic gateway linked to Atlantic water masses*

At the beginning of the drift station, the median integrated  $s_A$  (280-600 m) of the DSL at 38 kHz remained similar to previous mesopelagic values reported in the same area in August – September; a daily median of 182  $\text{m}^2 \text{nmi}^{-2}$  on June 4 compared to 45 – 148 in Knutsen et al.

(2017) and  $351 \text{ m}^2 \text{ nmi}^{-2}$  in Geoffroy et al. (2019). The backscatter within the DSL increased after June 5 and reached a daily median of  $7,871 \text{ m}^2 \text{ nmi}^{-2}$  on June 11, which is slightly higher than the range for mesopelagic DSL in tropical and subtropical areas ( $158\text{-}7,617 \text{ m}^2 \text{ nmi}^{-2}$ ; Irigoien et al., 2014). The backscatter continued to increase between June 12 and 15, over the eastern slope of the Yermak Plateau. There, the backscatter within the DSL reached a daily median of  $56,903 \text{ m}^2 \text{ nmi}^{-2}$  on June 13, which is higher than all mesopelagic backscatter values previously documented in the Arctic Ocean and north Atlantic (Fennell and Rose, 2015; Siegelman-Charbit and Planque, 2016; Gjørseter et al., 2017; Dias Bernardes et al., 2020; Snoeijs-Leijonmalm et al., 2021). The species likely forming the arctic DSL exhibit a denser aggregating behavior than lanternfish found in the north Atlantic. For instance, polar cod form dense aggregations at depth in the Atlantic water mass in the Beaufort Sea and the backscattering strength of these aggregations is similar to that measured over the slope of the Yermak Plateau (Benoit et al., 2010; Geoffroy et al., 2011). However, while the increase in backscattering strength can be related to an increase in mesopelagic biomass, it can also emerge from a change in species composition. Other potential contributors to the mesopelagic community at the Arctic-Atlantic gateway comprise macrozooplankton and gelatinous zooplankton (Knutsen et al., 2017; Geoffroy et al., 2019), including siphonophores (Raskoff et al., 2005).

The high backscattering strength observed within the DSL over the Yermak Plateau slope coincided with the regional AW circulation. On several occasions, the Yermak Branch that carries AW northward around the outer rim of the Yermak Plateau (Fig. 1) has been identified recirculating southward along the eastern slope of the plateau (Meyer et al., 2017; Crews et al., 2019; Athanase et al., 2020). The DSL backscatter increased where MAW thickened, which corresponds to the location where the Yermak Branch flows. Most mesopelagic fish encountered in the European Arctic are boreal species following their planktonic preys northward or advected with the inflow of Atlantic waters (Knutsen et al., 2017; Basedow et al., 2018; Geoffroy et al., 2019). Adult polar cod, the only abundant arctic pelagic fish, also often associate with warmer Atlantic waters (Geoffroy et al., 2011, 2016; Crawford et al., 2012). We thus suggest that the convergence and concentration of mesopelagic fish and plankton advected with Atlantic waters at least partly explain the spatial variation in mesopelagic backscatter, with backscatter two

orders of magnitude higher on the deeper continental slope of the Yermak Plateau than elsewhere.

## 5. Conclusion

In spring, mesopelagic organisms at the Arctic-Atlantic gateway can form aggregations with backscatter values comparable to or higher than in temperate regions. These mesopelagic organisms are concentrated in the Atlantic water masses. Hence, the increase in Atlantic water inflow into the Arctic (Athanasé et al., 2020) could likely result in an increased advection of mesopelagic biota. However, the fate of the advected mesopelagic species into the deep basins of the Arctic Oceans is unknown. The clear vertical segregation between mesopelagic animals and large epipelagic copepods in June, during the midnight sun period, suggests that mesopelagic fish can only feed on the lipid-rich copepod prey for a short period of time in early spring and fall. This confirms the very pulsed peaks in energy transfer prevailing in arctic marine ecosystems.

## References

- Athanasé, M., Provost, C., Artana, C., Pérez-Hernández, M.D., Sennéchaël, N., Bertosio, C., Garric, G., Lellouche, J.M., Prandi, P., 2021. Changes in Atlantic water circulation patterns and volume transports north of Svalbard over the last 12 years (2008–2020). *J. Geophys. Res. Ocean.* 126, 1–23. <https://doi.org/10.1029/2020JC016825>
- Basedow, S.L., Sundfjord, A., von Appen, W.J., Halvorsen, E., Kwasniewski, S., Reigstad, M., 2018. Seasonal variation in transport of zooplankton into the Arctic Basin through the Atlantic gateway, Fram Strait. *Front. Mar. Sci.* 5, 1–22. <https://doi.org/10.3389/fmars.2018.00194>
- Benoit, D., Simard, Y., Gagné, J., Geoffroy, M., Fortier, L., 2010. From polar night to midnight sun: photoperiod, seal predation, and the diel vertical migrations of polar cod (*Boreogadus saida*) under landfast ice in the Arctic Ocean. *Polar Biol.* 33, 1505–1520. <https://doi.org/10.1007/s00300-010-0840-x>

- Berge, J., Daase, M., Renaud, P.E., Ambrose, W.G., Darnis, G., Last, K.S., Leu, E., Cohen, J.H., Johnsen, G., Moline, M.A., Cottier, F., Varpe, O., Shunatova, N., Bałazy, P., Morata, N., Massabuau, J.C., Falk-Petersen, S., Kosobokova, K., Hoppe, C.J.M., Węślawski, J.M., Kukliński, P., Legeżyńska, J., Nikishina, D., Cusa, M., Kędra, M., Włodarska-Kowalczyk, M., Vogedes, D., Camus, L., Tran, D., Michaud, E., Gabrielsen, T.M., Granovitch, A., Gonchar, A., Krapp, R., Callesen, T.A., 2015. Unexpected levels of biological activity during the polar night offer new perspectives on a warming Arctic. *Curr. Biol.* 25, 2555–2561. <https://doi.org/10.1016/j.cub.2015.08.024>
- Berge, J., Geoffroy, M., Johnsen, G., Cottier, F., Bluhm, B., Vogedes, D., 2016. Ice-tethered observational platforms in the Arctic Ocean pack ice. *IFAC-PapersOnLine* 49, 494–499. <https://doi.org/10.1016/j.ifacol.2016.10.484>
- Bianchi, D., Galbraith, E.D., Carozza, D.A., Mislán, K.A.S., Stock, C.A., 2013. Intensification of open-ocean oxygen depletion by vertically migrating animals. *Nat. Geosci.* 6, 545–548. <https://doi.org/10.1038/ngeo1837>
- Blachowiak-Samolyk, K., Kwasniewski, S., Richardson, K., Dmoch, K., Hansen, E., Hop, H., Falk-Petersen, S., Mouritsen, L.T., 2006. Arctic zooplankton do not perform diel vertical migration (DVM) during periods of midnight sun. *Mar. Ecol. Prog. Ser.* 308, 101–116. <https://doi.org/10.3354/meps308101>
- Cade, D.E., Benoit-Bird, K.J., 2015. Depths, migration rates and environmental associations of acoustic scattering layers in the Gulf of California. *Deep. Res. Part I Oceanogr. Res. Pap.* 102, 78–89. <https://doi.org/10.1016/j.dsr.2015.05.001>
- Castellani, G., Schaafsma, F.L., Arndt, S., Lange, B.A., Peeken, I., Ehrlich, J., David, C., Ricker, R., Krumpfen, T., Hendricks, S., Schwegmann, S., Massicotte, P., Flores, H., 2020. Large-scale variability of physical and biological sea-ice properties in polar oceans. *Front. Mar. Sci.* 7, 1–22. <https://doi.org/10.3389/fmars.2020.00536>
- Cohen, J.H., Forward, R.B., 2009. Zooplankton diel vertical migration - a review of proximate control. *Oceanogr. Mar. Biol.* 47, 77–110. <https://doi.org/10.1201/9781420094220.ch2>
- Cottier, F.R., Tarling, G.A., Wold, A., Falk-Petersen, S., 2006. Unsynchronized and

- synchronized vertical migration of zooplankton in a high Arctic fjord. *Limnol. Oceanogr.* 51, 2586–2599. <https://doi.org/10.4319/lo.2006.51.6.2586>
- Crawford, R.E., Vagle, S., Carmack, E.C., 2012. Water mass and bathymetric characteristics of polar cod habitat along the continental shelf and slope of the Beaufort and Chukchi seas. *Polar Biol.* 35, 179–190. <https://doi.org/10.1007/s00300-011-1051-9>
- Crews, L., Sundfjord, A., Hattermann, T., 2019. How the Yermak Pass branch regulates Atlantic water inflow to the Arctic Ocean. *J. Geophys. Res. Ocean.* 124, 267–280. <https://doi.org/10.1029/2018JC014476>
- Daase, M., Eiane, K., 2007. Mesozooplankton distribution in northern Svalbard waters in relation to hydrography. *Polar Biol.* 30, 969–981. <https://doi.org/10.1007/s00300-007-0255-5>
- Daase, M., Hop, H., Falk-Petersen, S., 2016. Small-scale diel vertical migration of zooplankton in the high Arctic. *Polar Biol.* 39, 1213–1223. <https://doi.org/10.1007/s00300-015-1840-7>
- Dale, T., Bagøien, E., Melle, W., Kaartvedt, S., 1999. Can predator avoidance explain varying overwintering depth of *Calanus* in different oceanic water masses? *Mar. Ecol. Prog. Ser.* 179, 113–121. <https://doi.org/10.3354/meps179113>
- Darnis, G., Fortier, L., 2014. Temperature, food and the seasonal vertical migration of key arctic copepods in the thermally stratified Amundsen Gulf (Beaufort Sea, Arctic Ocean). *J. Plankton Res.* 36, 1092–1108. <https://doi.org/10.1093/plankt/fbu035>
- Darnis, G., Hobbs, L., Geoffroy, M., Grenvald, J.C., Renaud, P.E., Berge, J., Cottier, F., Kristiansen, S., Daase, M., E. Søreide, J., Wold, A., Morata, N., Gabrielsen, T., 2017. From polar night to midnight sun: diel vertical migration, metabolism and biogeochemical role of zooplankton in a high Arctic fjord (Kongsfjorden, Svalbard). *Limnol. Oceanogr.* 62, 1586–1605. <https://doi.org/10.1002/lno.10519>
- David, C., Lange, B., Krumpfen, T., Schaafsma, F., van Franeker, J.A., Flores, H., 2016. Under-ice distribution of polar cod *Boreogadus saida* in the central Arctic Ocean and their association with sea-ice habitat properties. *Polar Biol.* 39, 981–994. <https://doi.org/10.1007/s00300-015-1774-0>

- Davison, P.C., Checkley, D.M., Koslow, J.A., Barlow, J., 2013. Carbon export mediated by mesopelagic fishes in the northeast Pacific Ocean. *Prog. Oceanogr.* 116, 14–30. <https://doi.org/10.1016/j.pocean.2013.05.013>
- De Robertis, A., Higginbottom, I., 2007. A post-processing technique to estimate the signal-to-noise ratio and remove echosounder background noise. *ICES J. Mar. Sci.* 64, 1282–1291. <https://doi.org/10.1093/icesjms/fsm112>
- Demer, D.A., Berger, L., Bernasconi, M., Bethke, E., Boswell, K.M., Chu, D., Domokos, R., Dunford, A., Fassler, S., Gauthier, S., Hufnagle, L.T., Jech, J.M., Bouffant, N., Lebourges-Dhaussy, A., Lurton, X., Macaulay, G.J., Perrot, Y., Ryan, T., Parker-Stetter, S., Stienessen, S., Weber, T., Williamson, N., 2015. Calibration of acoustic instruments, International Council for the Exploration of the Sea (ICES) Cooperative Research Report No. 326. <https://doi.org/10.25607/OBP-185>
- Dias Bernardes, I., Ona, E., Gjørseter, H., 2020. Study of the Arctic mesopelagic layer with vessel and profiling multifrequency acoustics. *Prog. Oceanogr.* 182, 1–14. <https://doi.org/10.1016/j.pocean.2019.102260>
- Falk-Petersen, S., Mayzaud, P., Kattner, G., Sargent, J.R., 2009. Lipids and life strategy of Arctic *Calanus*. *Mar. Biol. Res.* 5, 18–39. <https://doi.org/10.1080/17451000802512267>
- Fennell, S., Rose, G., 2015. Oceanographic influences on deep scattering layers across the north Atlantic. *Deep. Res. Part I Oceanogr. Res. Pap.* 105, 132–141. <https://doi.org/10.1016/j.dsr.2015.09.002>
- Fortier, M., Fortier, L., Hattori, H., Saito, H., Legendre, L., 2001. Visual predators and the diel vertical migration of copepods under Arctic sea ice during the midnight sun. *J. Plankton Res.* 23, 1263–1278. <https://doi.org/10.1093/plankt/23.11.1263>
- Geoffroy, M., Daase, M., Cusa, M., Darnis, G., Graeve, M., Santana Hernández, N., Berge, J., Renaud, P.E., Cottier, F., Falk-Petersen, S., 2019. Mesopelagic sound scattering layers of the high Arctic: seasonal variations in biomass, species assemblage, and trophic relationships. *Front. Mar. Sci.* 6, 1–18. <https://doi.org/10.3389/fmars.2019.00364>
- Geoffroy, M., Majewski, A., LeBlanc, M., Gauthier, S., Walkusz, W., Reist, J.D., Fortier, L.,

2016. Vertical segregation of age-0 and age-1+ polar cod (*Boreogadus saida*) over the annual cycle in the Canadian Beaufort Sea. *Polar Biol.* 39, 1023–1037.  
<https://doi.org/10.1007/s00300-015-1811-z>
- Geoffroy, M., Robert, D., Darnis, G., Fortier, L., 2011. The aggregation of polar cod (*Boreogadus saida*) in the deep Atlantic layer of ice-covered Amundsen Gulf (Beaufort Sea) in winter. *Polar Biol.* 34, 1959–1971. <https://doi.org/10.1007/s00300-011-1019-9>
- Gjørseter, H., Ingvaldsen, R., Christiansen, J.S., 2020. Acoustic scattering layers reveal a faunal connection across the Fram Strait. *Prog. Oceanogr.* 185, 1–11.  
<https://doi.org/10.1016/j.pocean.2020.102348>
- Gjørseter, H., Wiebe, P.H., Knutsen, T., Ingvaldsen, R.B., 2017. Evidence of diel vertical migration of mesopelagic sound-scattering organisms in the Arctic. *Front. Mar. Sci.* 4, 1–14. <https://doi.org/10.3389/fmars.2017.00332>
- Gostiaux, L., van Haren, H., 2010. Extracting meaningful information from uncalibrated backscattered echo intensity data. *J. Atmos. Ocean. Technol.* 27, 943–949.  
<https://doi.org/10.1175/2009JTECHO704.1>
- Hays, G.C., 2003. A review of the adaptive significance and ecosystem consequences of zooplankton diel vertical migrations. *Hydrobiologia* 503, 163–170.  
<https://doi.org/10.1023/B:HYDR.0000008476.23617.b0>
- Hirche, H.J., Muyakshin, S., Klages, M., Auel, H., 2006. Aggregation of the Arctic copepod *Calanus hyperboreus* over the ocean floor of the Greenland Sea. *Deep. Res. Part I Oceanogr. Res. Pap.* 53, 310–320. <https://doi.org/10.1016/j.dsr.2005.08.005>
- Ingvaldsen, R.B., Gjørseter, H., Ona, E., Michalsen, K., 2017. Atlantic cod (*Gadus morhua*) feeding over deep water in the high Arctic. *Polar Biol.* 40, 2105–2111.  
<https://doi.org/10.1007/s00300-017-2115-2>
- Irigoiien, X., Klevjer, T.A., Røstad, A., Martinez, U., Boyra, G., Acuña, J.L., Bode, A., Echevarria, F., Gonzalez-Gordillo, J.I., Hernandez-Leon, S., Agusti, S., Aksnes, D.L., Duarte, C.M., Kaartvedt, S., 2014. Large mesopelagic fishes biomass and trophic efficiency in the open ocean. *Nat. Commun.* 5, 1–10. <https://doi.org/10.1038/ncomms4271>

- Kaartvedt, S., 2008. Photoperiod may constrain the effect of global warming in Arctic marine systems. *J. Plankton Res.* 30, 1203–1206. <https://doi.org/10.1093/plankt/fbn075>
- Katlein, C., Schiller, M., Belter, H.J., Coppolaro, V., Wenslandt, D., Nicolaus, M., 2017. A new remotely operated sensor platform for interdisciplinary observations under sea ice. *Front. Mar. Sci.* 4, 1–12. <https://doi.org/10.3389/fmars.2017.00281>
- Klevjer, T.A., Irigoien, X., Røstad, A., Fraile-Nuez, E., Benítez-Barrios, V.M., Kaartvedt, S., 2016. Large scale patterns in vertical distribution and behaviour of mesopelagic scattering layers. *Sci. Rep.* 6, 1–11. <https://doi.org/10.1038/srep19873>
- Knutsen, T., Wiebe, P.H., Gjørseter, H., Ingvaldsen, R.B., Lien, G., 2017. High latitude epipelagic and mesopelagic scattering layers - a reference for future Arctic ecosystem change. *Front. Mar. Sci.* 4, 1–21. <https://doi.org/10.3389/fmars.2017.00334>
- Korneliussen, R.J., Berger, L., Campanila, F., Chu, D., Demer, D.A., De Robertis, A., Domokos, R., Doray, M., Fielding, S., Fässler, S., Gauthier, S., Gastauer, S., Horne, J.K., Hutton, B., Iriarte, F., Jech, J.M., Kloser, R.J., Lawson, G.L., Lebourges-Dhaussy, A., McQuinn, I., Peña, M., Scoulding, B., Sakinan, S., Schaber, M., Taylor, J.C., Thompson, C.H., 2018. Acoustic target classification, International Council for the Exploration of the Sea (ICES) Cooperative Research Report No. 344. <https://doi.org/10.17895/ices.pub.4567>
- Kosobokova, K.N., Hopcroft, R.R., 2010. Diversity and vertical distribution of mesozooplankton in the Arctic's Canada Basin. *Deep. Res. Part II Top. Stud. Oceanogr.* 57, 96–110. <https://doi.org/10.1016/j.dsr2.2009.08.009>
- Langbehn, T.J., Aksnes, D.L., Kaartvedt, S., Fiksen, Ø., Jørgensen, C., 2019. Light comfort zone in a mesopelagic fish emerges from adaptive behaviour along a latitudinal gradient. *Mar. Ecol. Prog. Ser.* 623, 161–174. <https://doi.org/10.3354/meps13024>
- Meyer, A., Sundfjord, A., Fer, I., Provost, C., Villacieros Robineau, N., Koenig, Z., Onarheim, I.H., Smedsrud, L.H., Duarte, P., Dodd, P.A., Graham, R.M., Schmidtko, S., Kauko, H.M., 2017. Winter to summer oceanographic observations in the Arctic Ocean north of Svalbard. *J. Geophys. Res. Ocean.* 122, 6218–6237. <https://doi.org/10.1002/2016JC012391>
- Münchow, A., Falkner, K.K., Melling, H., 2015. Baffin Island and west Greenland current

- systems in northern Baffin Bay. *Prog. Oceanogr.* 132, 305–317.  
<https://doi.org/10.1016/j.pocean.2014.04.001>
- Naito, Y., Costa, D.P., Adachi, T., Robinson, P.W., Fowler, M., Takahashi, A., 2013.  
Unravelling the mysteries of a mesopelagic diet: a large apex predator specializes on small prey. *Funct. Ecol.* 27, 710–717. <https://doi.org/10.1111/1365-2435.12083>
- Norheim, E., Klevjer, T.A., Aksnes, D.L., 2016. Evidence for light-controlled migration amplitude of a sound scattering layer in the Norwegian Sea. *Mar. Ecol. Prog. Ser.* 551, 45–52. <https://doi.org/10.3354/meps11731>
- Pearre, S., 2003. Eat and run? The hunger/satiation hypothesis in vertical migration: history, evidence and consequences. *Biol. Rev. Camb. Philos. Soc.* 78, 1–79.  
<https://doi.org/10.1017/S146479310200595X>
- Peña, M., Cabrera-Gómez, J., Domínguez-Brito, A.C., 2020. Multi-frequency and light-avoiding characteristics of deep acoustic layers in the north Atlantic. *Mar. Environ. Res.* 154, 1–9.  
<https://doi.org/10.1016/j.marenvres.2019.104842>
- Perovich, D.K., 2005. On the aggregate-scale partitioning of solar radiation in Arctic sea ice during the Surface Heat Budget of the Arctic Ocean (SHEBA) field experiment. *J. Geophys. Res. C Ocean.* 110, 1–12. <https://doi.org/10.1029/2004JC002512>
- Proud, R., Cox, M.J., Brierley, A.S., 2017. Biogeography of the global ocean’s mesopelagic zone. *Curr. Biol.* 27, 113–119. <https://doi.org/10.1016/j.cub.2016.11.003>
- Raskoff, K.A., Purcell, J.E., Hopcroft, R.R., 2005. Gelatinous zooplankton of the Arctic Ocean: *in situ* observations under the ice. *Polar Biol.* 28, 207–217. <https://doi.org/10.1007/s00300-004-0677-2>
- Røstad, A., Kaartvedt, S., Aksnes, D.L., 2016. Light comfort zones of mesopelagic acoustic scattering layers in two contrasting optical environments. *Deep. Res. Part I Oceanogr. Res. Pap.* 113, 1–6. <https://doi.org/10.1016/j.dsr.2016.02.020>
- Ryan, T.E., Downie, R.A., Kloser, R.J., Keith, G., 2015. Reducing bias due to noise and attenuation in open-ocean echo integration data. *ICES J. Mar. Sci.* 72, 2482–2493.  
<https://doi.org/10.1093/icesjms/fsv121>

- Sameoto, D., 1989. Feeding ecology of the lantern fish *Benthoosema glaciale* in a subarctic region. *Polar Biol.* 9, 169–178. <https://doi.org/10.1007/BF00297172>
- Saunders, R.A., Hill, S.L., Tarling, G.A., Murphy, E.J., 2019. Myctophid fish (Family Myctophidae) are central consumers in the food web of the Scotia Sea (Southern Ocean). *Front. Mar. Sci.* 6, 1–22. <https://doi.org/10.3389/fmars.2019.00530>
- Siegelman-Charbit, L., Planque, B., 2016. Abundant mesopelagic fauna at oceanic high latitudes. *Mar. Ecol. Prog. Ser.* 546, 277–282. <https://doi.org/10.3354/meps11661>
- Snoeijs-Leijonmalm, P., Gjørseter, H., Ingvaldsen, R.B., Knutsen, T., Korneliussen, R., Ona, E., Rune Skjoldal, H., Stranne, C., Mayer, L., Jakobsson, M., Gårdfeldt, K., 2021. A deep scattering layer under the North Pole pack ice. *Prog. Oceanogr.* 194, 1–14. <https://doi.org/10.1016/j.pocean.2021.102560>
- Urmy, S.S., Horne, J.K., Barbee, D.H., 2012. Measuring the vertical distributional variability of pelagic fauna in Monterey Bay. *ICES J. Mar. Sci.* 69, 184–196. <https://doi.org/10.1093/icesjms/fsr205>
- Wollenburg, J.E., Iversen, M., Katlein, C., Krumpen, T., Nicolaus, M., Castellani, G., Peeken, I., Flores, H., 2020. New observations of the distribution, morphology and dissolution dynamics of cryogenic gypsum in the Arctic Ocean. *Cryosphere* 14, 1–14. <https://doi.org/10.5194/tc-14-1795-2020>
- Wood, S.N., 2017. Generalized additive models: an introduction with R, 2nd Editio. ed. Chapman and Hall/CRC, New York. <https://doi.org/10.1201/9781315370279>
- Zolich, A., De La Torre, P.R., Rodwell, S., Geoffroy, M., Johnsen, G., Berge, J., 2019. An ice-tethered buoy for fish and plankton research, in: OCEANS 2018 MTS/IEEE Charleston, OCEAN 2018. pp. 1–7. <https://doi.org/10.1109/OCEANS.2018.8604603>

### Author contributions

PP led the analyses of the ice-tethered and ship-based acoustic datasets and writing of the manuscript. AN and TL led the ice-tethered ADCP and ship CTD deployments and analyses. RG

and EK led the ice-tethered AZFPs deployment. CK conducted the ROV, irradiance, and snow buoy deployment. HF led the ROVnet deployment and zooplankton analyses. GC contributed to the ROVnet deployment and conducted the deployment of the handheld CTD from the ice floe. JB and MG designed the study. JF contributed substantially to drafting the manuscript. All co-authors contributed to writing and reviewing the manuscript.

### **Declaration of competing interests**

The authors declare that they have no known competing financial interests or personal relationships that could have appeared to influence the work reported in this paper.

### **Acknowledgments**

We thank the officers and crew of the R/V *Polarstern* and the numerous colleagues who helped during the PS106.1 expedition. We also acknowledge the very dedicated work of Daniel Vogedes and Pedro De La Torre for the development of the ice-tethered sensors, the help of Eric Pedersen while developing the GAMS, Marcel Nicolaus for his contribution with ROV work and under-ice irradiance data, and Marylou Athanase who provided valuable knowledge about regional AW circulation. This study used samples and data provided by the Alfred-Wegener-Institut Helmholtz-Zentrum für Polar- und Meeresforschung from R/V *Polarstern* expedition PS 106 (AWI-PS106\_00). This research was funded by the Helmholtz Association through the Young Investigators Group Iceflux (VH-NG-800), the infrastructure initiative FRAM (Frontiers in Arctic marine Monitoring), the PACES II (Polar Regions and Coasts in a Changing Earth System) and POF IV programs, by the UK-German Research initiative “Changing Arctic Ocean” with the projects EcoLight (03V01465), Diatom ARCTIC (NE/R012849/1; 03F0810A), and Coldfish (03F0800A), by three grants from the Norwegian Research Council: Arctic ABC Development (245923), Deep Impact (300333), and the Centre of Excellence AMOS (223254), one grant from Tromsø Forskningsstiftelse (TFS project ID 18 Arctic ABC East) and by the Ocean Frontier Institute through the Canada First Research Excellence fund. Grants to M. Geoffroy from the Natural Sciences and Engineering Research Council, ArcticNet a Network of Centres of Excellence Canada, and Atlantic Fisheries Fund supported this research. R. Gradinger

was supported by Arctic SIZE, a project co-funded by UiT The Arctic University of Norway and the Tromsø Research Foundation (01vm/h15). This is a contribution to the ARCTOS research network (arctos.uit.no) and to the Arctic Science Partnership (www.asp-net.org).

### Appendix A. Supplementary material

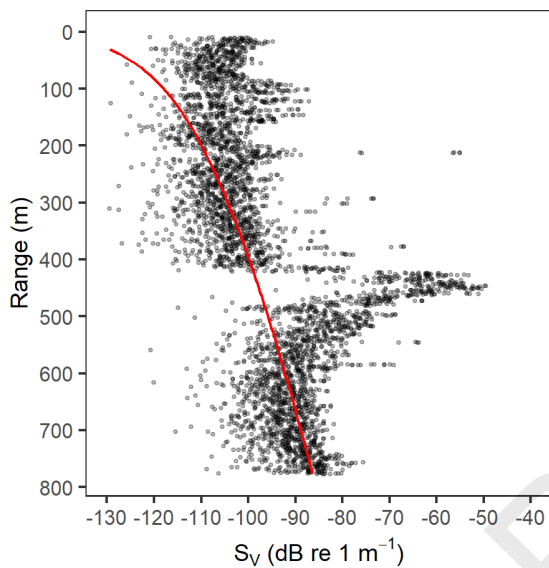


Fig. S1. Example of raw  $S_V$  profile (black dots) of a single ping collected on June 06, 2017 at 06:07:27 UTC at 38 kHz from the hull-mounted EK60. The red curve shows the time varied gain function with a noise estimate of -160 dB at 1 m of the transducer. The peak in  $S_V$  between 600 and 500 m depth originates from the DSL.

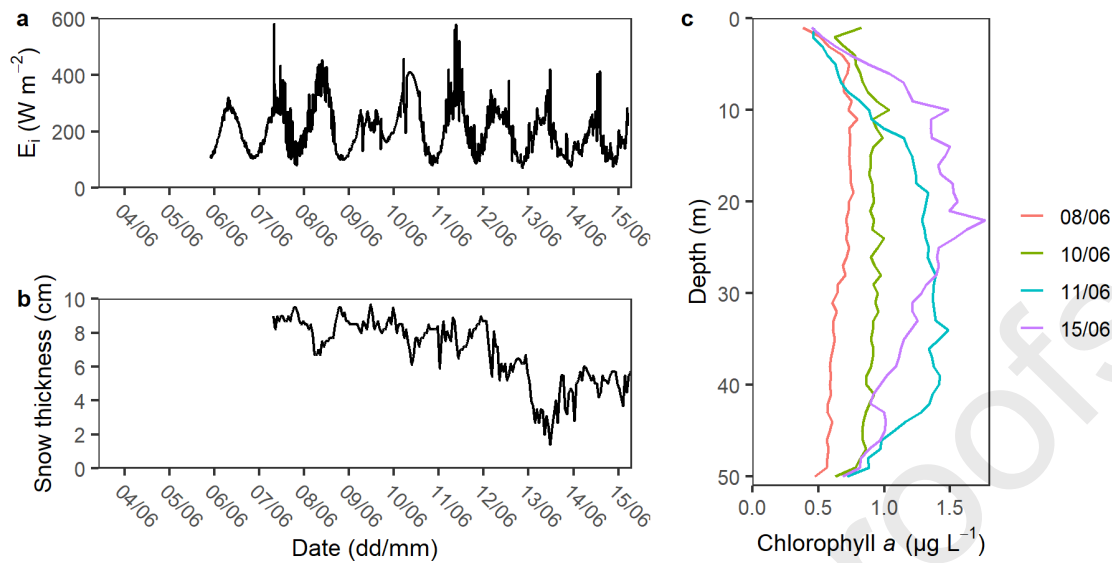


Fig. S2. (a) Above-ice irradiance ( $E_i$  in  $\text{W m}^{-2}$ ), (b) snow thickness measured at the surface of the ice floe, and (c) chlorophyll  $a$  profiles from the top 50 m as measured by the handheld CTD deployed from the ice floe.

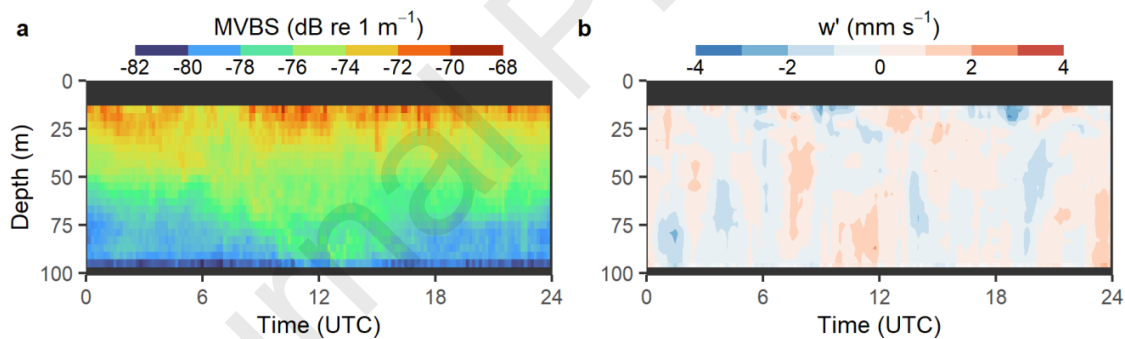


Fig. S3. Mean 24 h composites of (a) mean volume backscattering strength (MVBS) and (b) vertical velocity anomalies ( $w'$ ) from the ice-tethered ADCP at 307.2 kHz between June 5-15. Net upward velocities (positive) are denoted by red contours and net downward velocities (negative) by blue contours. For vertical velocity anomalies, days when the tilt of the ADCP was changing too quickly were excluded (June 7, 10, and 11).

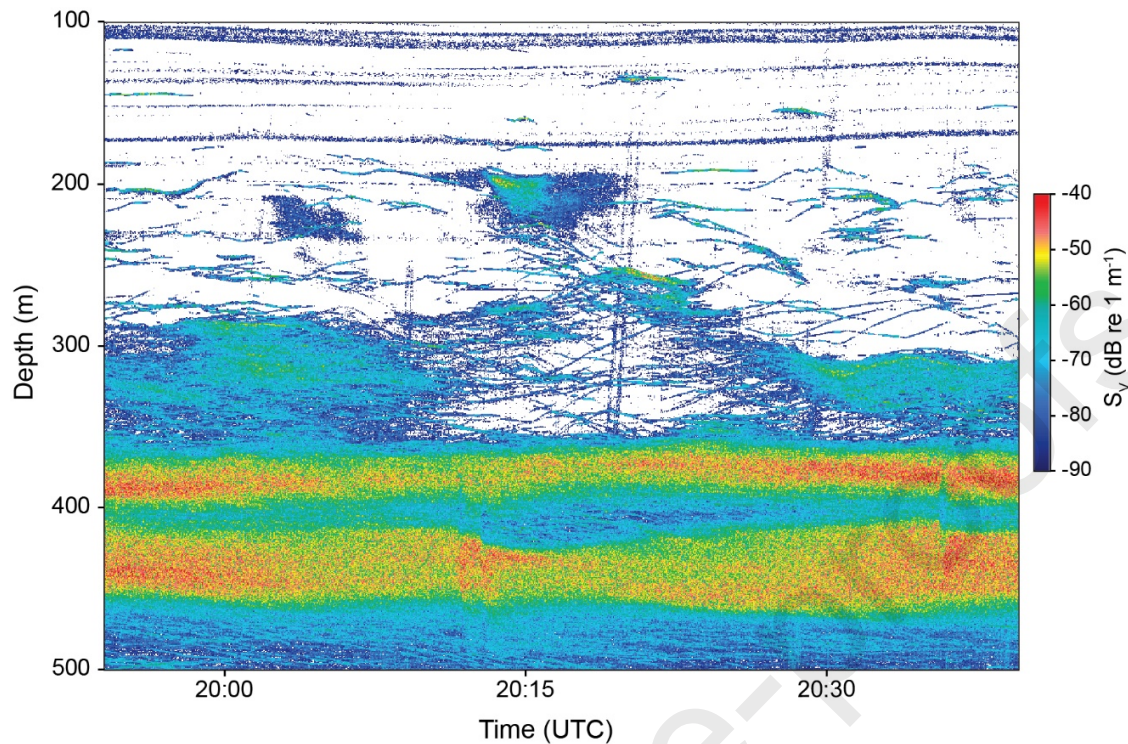


Fig. S4. Example of an echogram of denoised  $S_V$  at 38 kHz from the hull-mounted EK60 on June 14, 2017, showing the inter-connection between scattered intermediate patches and the DSL. Single echoes can be seen migrating between the patches and the DSL.

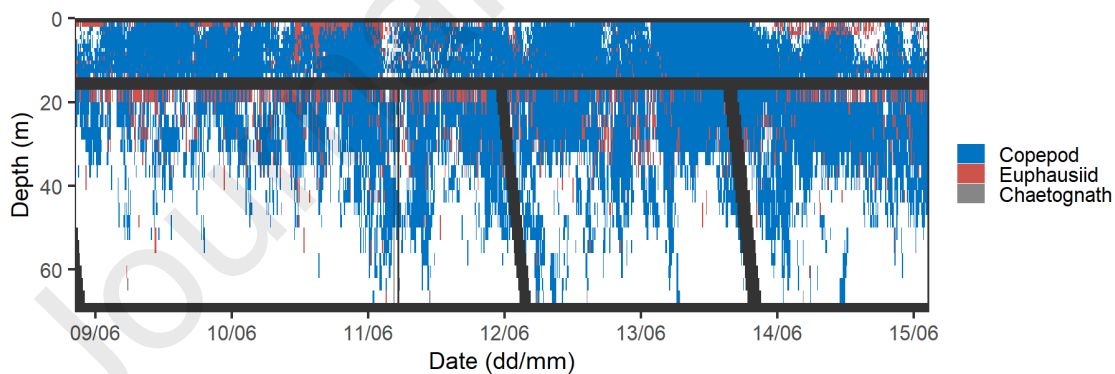


Fig. S5. Echogram from the ice-tethered AZFP with echo-integration cell classified as copepod (blue), euphausiid (red), and chaetognath (grey) based on the multifrequency criterion of Darnis et al. (2017). Empty water is depicted in white and area with bad acoustic data (due to acoustic interference with other instruments, near-field, or dead zone near the sea ice) or with no data are black.

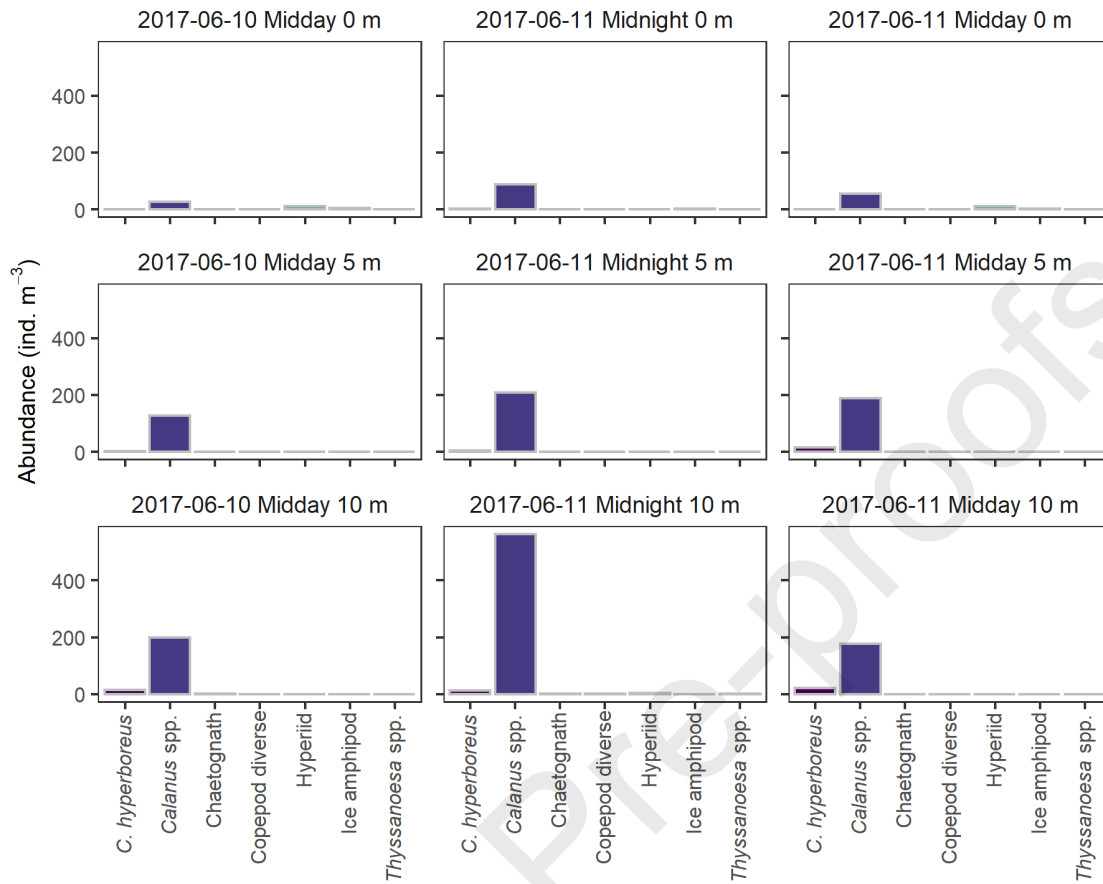


Fig. S6. Mesozooplankton abundance at 0, 5, and 10 m under the ice collected by the ROVnet.

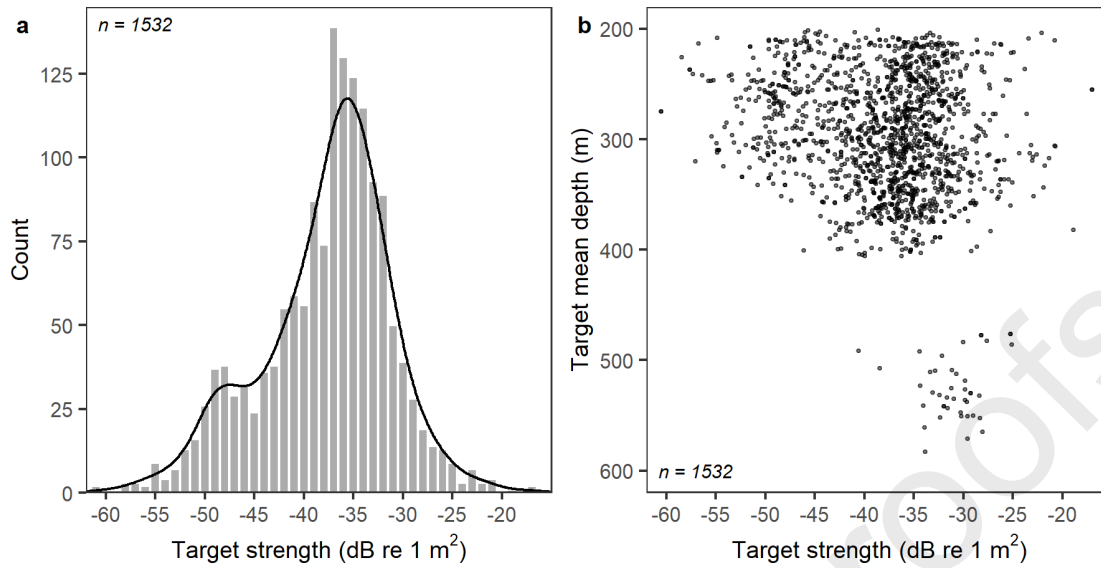


Fig. S7. **(a)** Target strength histogram and kernel density curve (black line, bandwidth of 1.65) from single target tracks, i.e., single target tracked over at least 5 consecutive pings, between 200 and 600 m depth at 38 kHz. **(b)** Corresponding depth distribution of the single target tracks detected at 38 kHz between 200 and 600 m depth.

Table S1. Settings of the different echosounders used during the drift station. \* The 18 kHz transducer was not calibrated; <sup>a</sup> the pulse length of the 70 kHz transducer was increased from 0.512 ms to 1.024 ms on June 9 at 12:30 UTC; <sup>b</sup> the pulse length of the 120 and 200 kHz was increased from 0.256 ms to 1.024 ms on June 9 at 12:30 UTC.

<b>Echosounder</b>	<b>Frequency</b> kHz	<b>Pulse length</b> ms	<b>Ping rate</b> Hz	<b>Beam width</b> °	<b>Gain</b> dB	<b>Nominal source level</b> dB re 1 μPa	<b>Transmitting power</b> W
AZFP upward	38	0.500	0.5	12		208	23.9
AZFP upward	125	0.190	0.5	8		210	13.7
AZFP upward	200	0.170	0.5	8		210	14.3
AZFP upward	455	0.130	0.5	7		210	10.6
AZFP downward	38	1.000	0.25	12		208	23.9
AZFP downward	125	1.000	0.25	8		210	13.7
AZFP downward	200	1.000	0.25	8		210	14.3
AZFP downward	455	1.000	0.25	7		210	10.6
EK60	18*	1.024	~ 0.5	11			1000
EK60	38	1.024	~ 0.5	7	24.84		1000
EK60	70 <sup>a</sup>	0.512/1.024	~ 0.5	7	25.78		750
EK60	120 <sup>b</sup>	0.256/1.024	~ 0.5	7	24.54		250
EK60	200 <sup>b</sup>	0.256/1.024	~ 0.5	7	24.58		150

Table S2. Parameters of Echoview single-echo detection algorithm for split beam echosounder (method 2) used to isolate single targets.

<b>Parameters</b>	<b>Values</b>
Compensated TS threshold (dB)	-100.0
Pulse length determination level (dB)	6.0
Minimum normalized pulse length	0.7
Maximum normalized pulse length	1.5
Beam compensation model	Simrad LOBE
Maximum beam compensation (dB)	3.0
Maximum standard deviation of minor-axis angles (°)	1.0
Maximum standard deviation of major-axis angles (°)	1.0

Table S3. Parameters of Echoview fish tracking algorithm used to detect single target tracks (named fish tracks in Echoview). Here, we tracked single targets over 5 consecutive pings with no missed detection between pings. Only single targets found to be within a maximum diameter of 2 m (athwartship and alongship) and 1 m range single targets from their position at the previous ping were retained.

<b>Parameters</b>	<b>Values</b>		
<i>Data</i>	4D (range, angles and time)		
<i>Weights</i> - Major axis	30		
<i>Weights</i> - Minor axis	40		
<i>Weights</i> - Range	40		
<i>Weights</i> - TS	0		
<i>Weights</i> - ping gap	3		
<i>Track acceptance</i> – Min. number of single targets in a track	5		
<i>Track acceptance</i> – Min. number of pings in track	5		
<i>Track acceptance</i> – Max. gap between single targets (pings)	0		
	<b>Major axis (Athw.)</b>	<b>Minor axis (Along.)</b>	<b>Range</b>
<i>Track detection</i> - Alpha	0.7	0.7	0.7
<i>Track detection</i> - Beta	0.5	0.5	0.5
<i>Target gates</i> - Exclusion distance (m)	2	2	1
<i>Target gates</i> - Missed ping expansion (%)	0	0	0

Table S4. Model fit statistics and parameter estimates for the generalized additive models (GAM) used to examine the relationship between the weighted mean depth (WMD in m) or backscatter intensity ( $s_A$  in dB re 1 m<sup>2</sup> nmi<sup>-2</sup>) and environmental drivers for the SSL and DSL. Environmental drivers include bottom depth (Bot.), temperature of polar surface water ( $T_{psw}$ ), temperature of modified Atlantic water ( $T_{MAW}$ ), and the tensor product of under-ice irradiance ( $E_d$ ) and time of day. Significant drivers are highlighted in grey ( $p$ -value < 0.05).

	Model intercept		Smooth terms			Model metrics	
			s(Bot.)	s( $T_{psw}$ )	s( $T_{MAW}$ )	te(time, $E_d$ )	
<b>SSL</b>	WMD	Estimate 30.9	edf 3.687			7.669	$r^2$ adj. 0.63
		t-value 109.4	F 23.970			3.545	AR(1) 0.77
		p >  t  < 0.001	p-value < 0.001			< 0.001	Num. obs. 777
log <sub>10</sub> ( $s_A$ )		Estimate 1.4	edf 2.460				$r^2$ adj. 0.43
		t-value 120.7	F 15.714				AR(1) 0.83
		p >  t  < 0.001	p-value < 0.001				Num. obs. 777
WMD		Estimate 416.9	edf 2.696		3.452		$r^2$ adj. 0.34
		t-value 512.6	F 6.736		3.350		AR(1) 0.68
		p >  t  < 0.001	p-value < 0.001		0.006		Num. obs. 1207
<b>DSL</b>		Estimate 4.0	edf 3.678				$r^2$ adj. 0.70
		t-value 222.5	F 68.463				AR(1) 0.71
		p >  t  < 0.001	p-value < 0.001				Num. obs. 1207

### **Declaration of competing interests**

The authors declare that they have no known competing financial interests or personal relationships that could have appeared to influence the work reported in this paper.

Journal Pre-proof

## Highlights

- Mesopelagic animals formed a deep scattering layer at the Arctic-Atlantic gateway
- Segregation of epi- and mesopelagic animals under sea ice during the midnight sun
- Higher mesopelagic backscattering strength than previously reported in the Arctic
- Link between mesopelagic backscattering strength and Atlantic water circulation

Journal Pre-proofs